TURBULENT DYNAMO IN BINARY NEUTRON STAR MERGERS

Daniele Viganò
Ricard Aguilera-Miret, Carlos Palenzuela,
Federico Carrasco, Borja Miñano

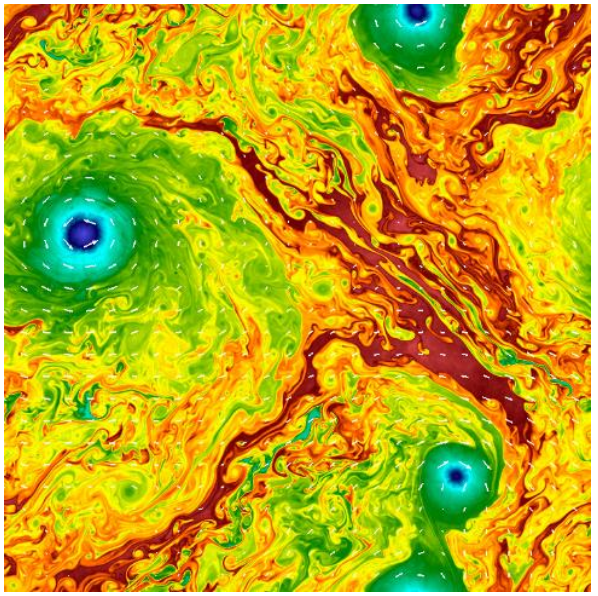

SISSA Trieste 8th October 2020

Computational resources:
«LESBNS» project (20th PRACE Regular Call)
MareNostrum BSC

PRACE

UIB Universitat de les Illes Balears

IAC3 Institute of Applied Computing & Community Code.

Institute of Space Sciences

CSIC Consejo Superior de Investigaciones Científicas

IEEC

Modeling MHD turbulence

2020arXiv200906669A 2020/09 cited: 1

Turbulent magnetic-field amplification in the first 10 milliseconds after a binary neutron star merger: comparing high-resolution and large eddy simulations

Aguilera-Miret, Ricard; Viganò, Daniele; Carrasco, Federico *and 2 more*

2020PhRvD.101l3019V 2020/06 cited: 1

General relativistic MHD large eddy simulations with gradient subgrid-scale model

Viganò, Daniele; Aguilera-Miret, Ricard; Carrasco, Federico *and 2 more*

2020PhRvD.101f3003C 2020/03 cited: 5

Gradient subgrid-scale model for relativistic MHD large-eddy simulations

Carrasco, Federico; Viganò, Daniele; Palenzuela, Carlos

2019PhFl...31j5102V 2019/10 cited: 5

Extension of the subgrid-scale gradient model for compressible magnetohydrodynamics turbulent instabilities

Viganò, Daniele; Aguilera-Miret, Ricard; Palenzuela, Carlos

Binary neutron star mergers

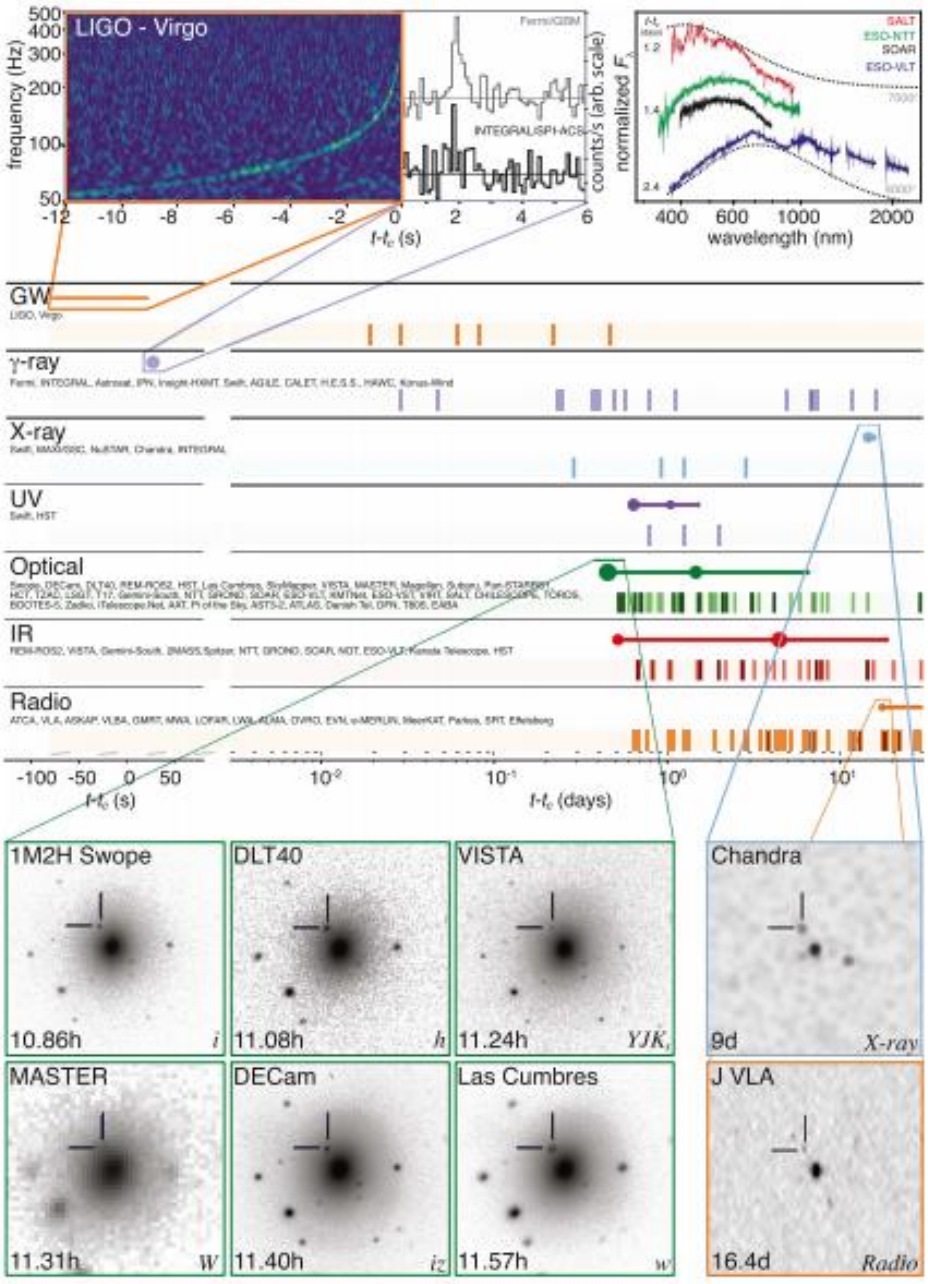

GW 170817:
the beginning of the multi-messenger era

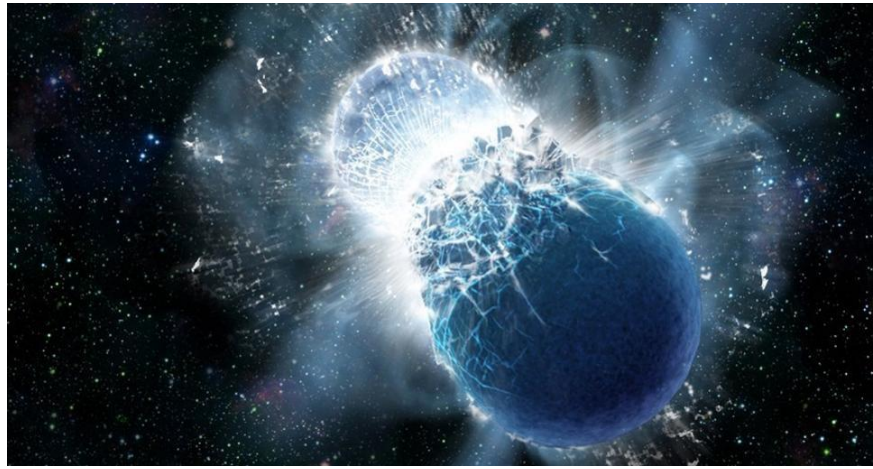

Binary neutron star mergers

RELEVANCE:

- General Relativity
- Internal properties of NSs (eq. state)
- **Magnetic amplification mechanism**
- Production of heavy elements
- EM counterpart (short GRB, kilonova)
- Formation of massive NS and light BH
- …

GW 170817:
the beginning of the multi-messenger era

A lucky event? Short distance (40 Mpc) + favourable geometry

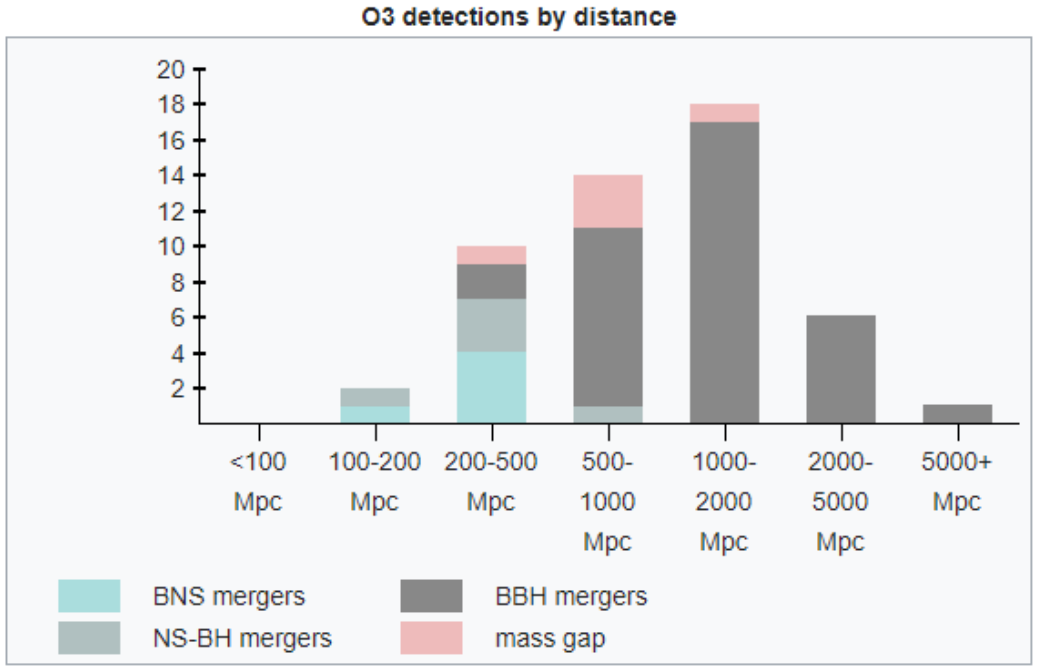

Constraining EoS (maximum mass, radius…)

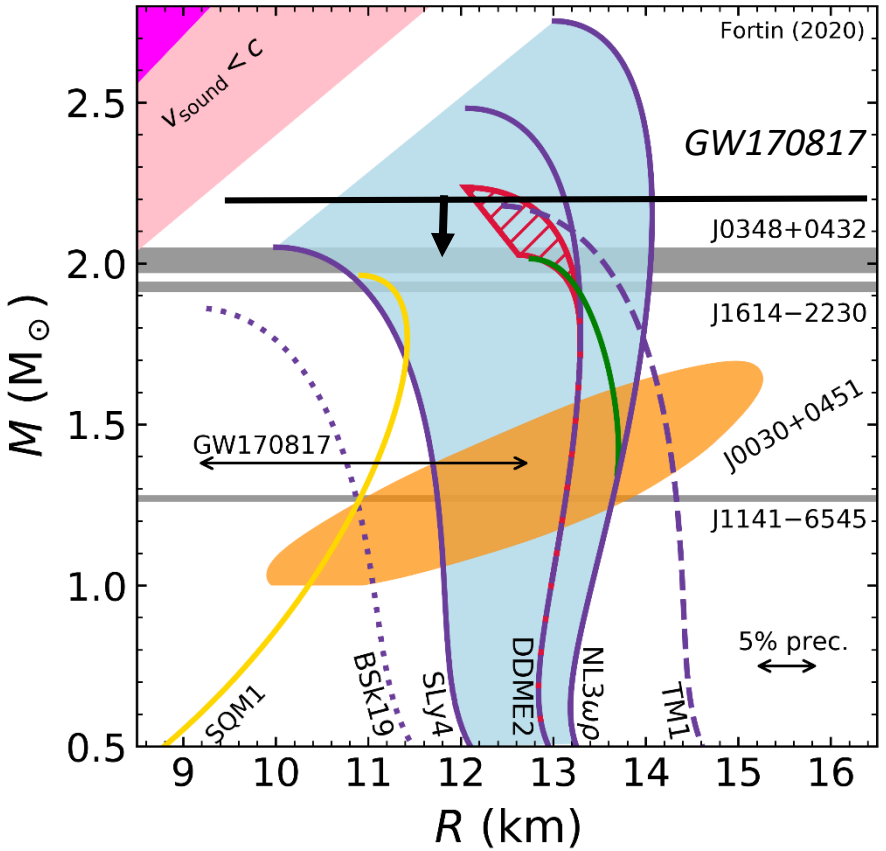

[adapted from Fortin 2020]

Different groups have inferred a maximum mass for cold non-rotating neutron stars of about 2.2 solar masses under the assumption of a collapse of the remnant to a Black Hole [see Godzieba+ 2020 and refs within]

More indirect estimates also for radius [Bauswein+ 2017]

The role of magnetic fields in mergers

PROCESSES DURING AND AFTER THE MERGER:

- Kelvin-Helmholtz instability: more effective at small scales, currently not resolvable (below meters)
- Winding (large scale)
- Magneto-rotational instability (large scale)

IMPRINTS OF A **LARGE-SCALE** MAGNETIC FIELD:

- **Effective viscous effect** on the angular momentum transportation => **Fate of the remnant** [Shibata's group series of works]
- Jet formation and ejected mass
- Possible formation of **millisecond magnetars?**

Invited Review: State of the Field | Published: 19 June 2020

The key role of magnetic fields in binary neutron star mergers

Riccardo Ciolfi

General Relativity and Gravitation **52**, Article number: 59 (2020) | Cite this article

High-resolution GRMHD simulations of mergers

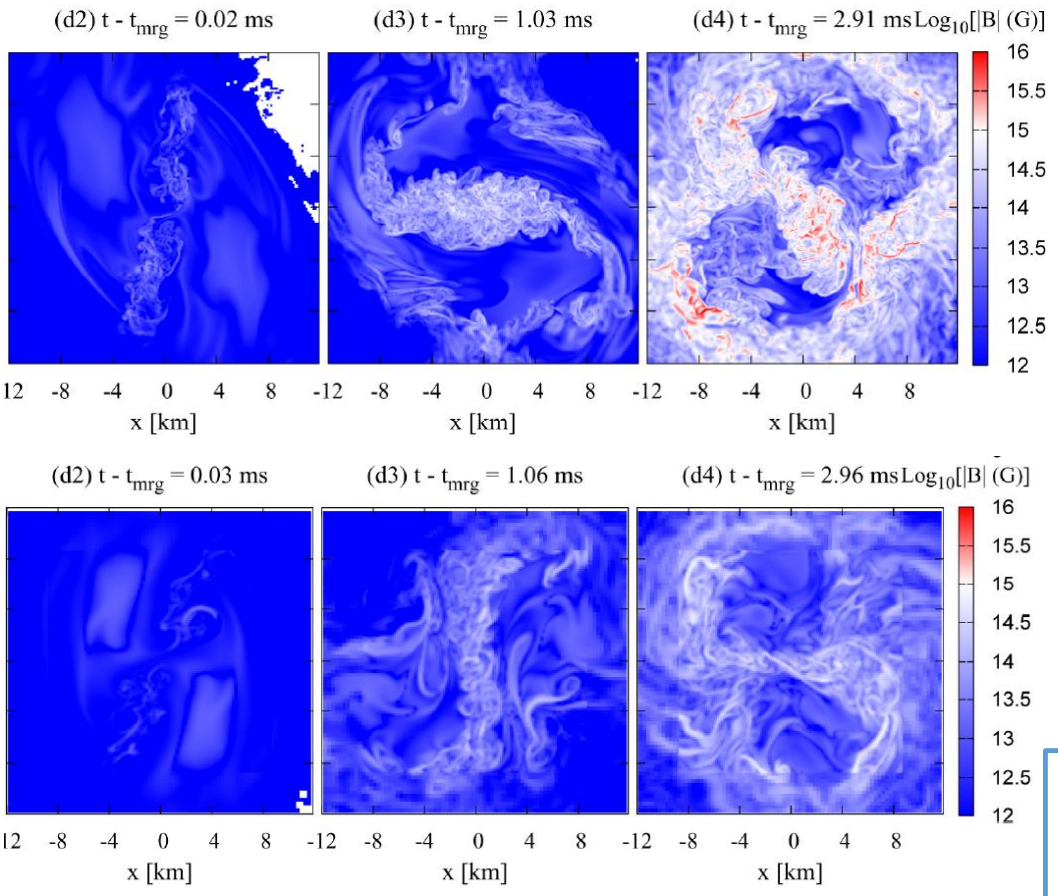

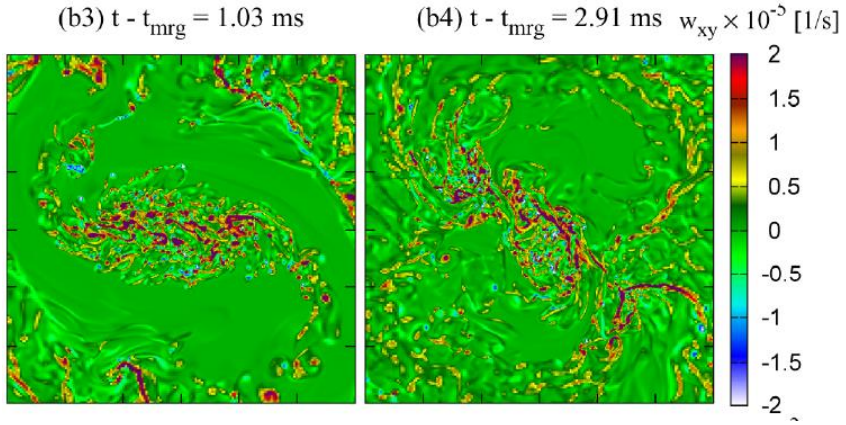

[Kiuchi+ 2015,2018]

Big difference between
dx = 17.5 m (top) and
dx = 37 m (bottom)

They see amplification at small scales, then MRI+winding to form a large-scale MF.
But: **Huge initial large-scale dipolar field B = 10^{15} G** (in order to solve MRI)

Long simulations

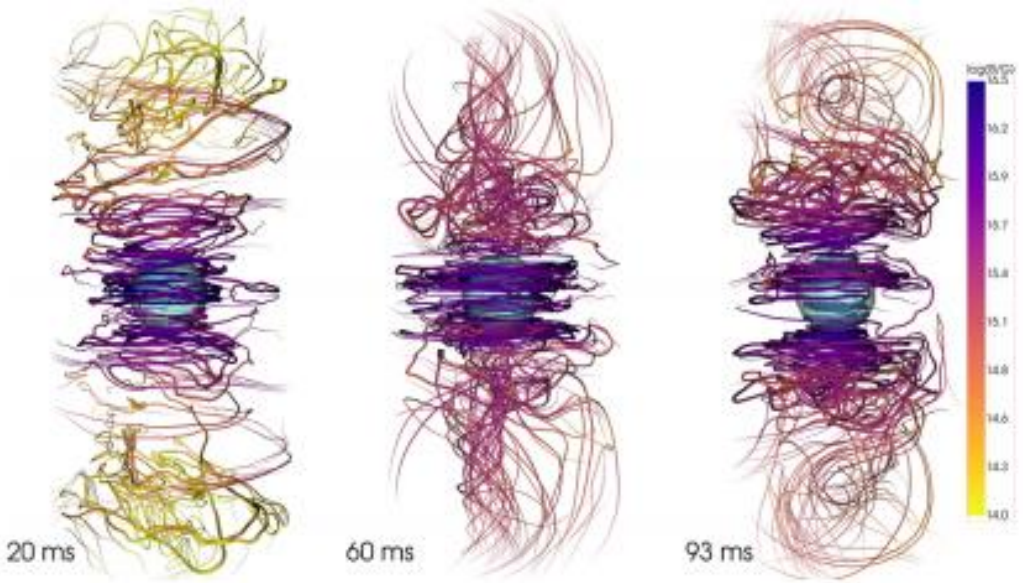

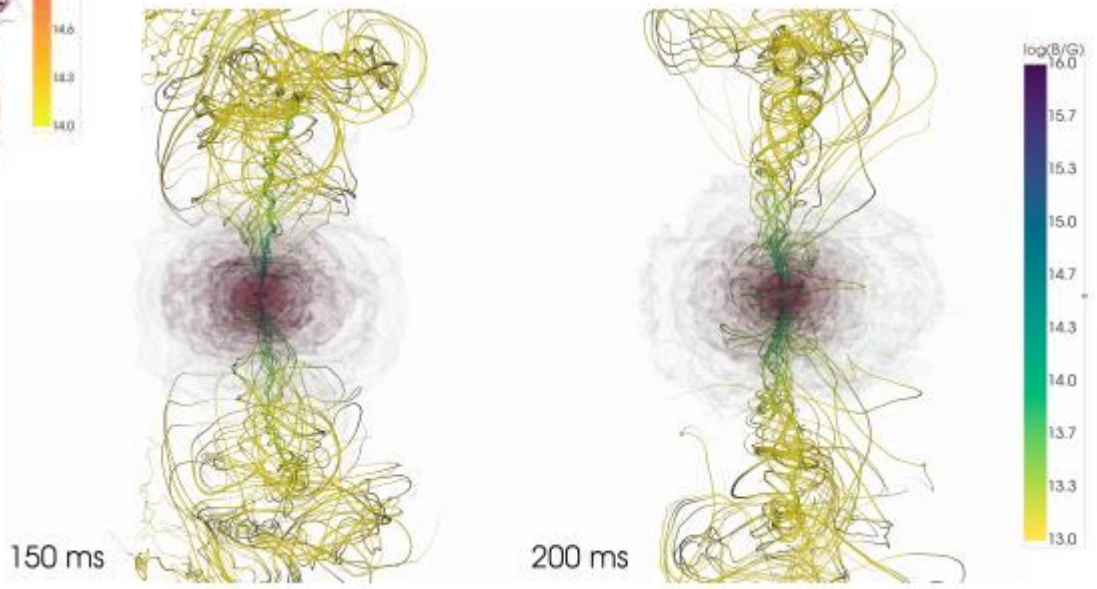

[Ciolfi+ 2019, Ciolfi 2020]

Remnant not collapsed, jet is formed but insufficient to power a short GRB
(but: no neutrinos)

Jet formation

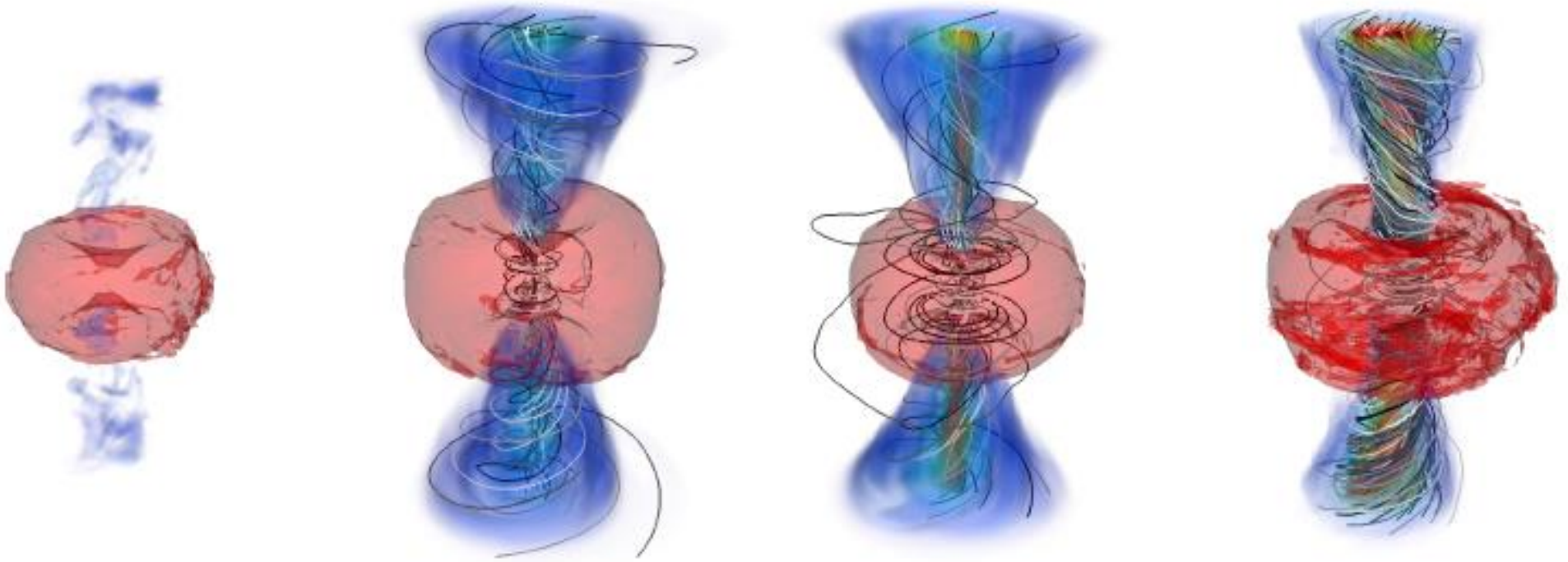

Figure 5. Volume renderings of the Bernoulli criterion (blue colormap) indicating unbound material and the disk contour at $\rho = 10^{10}\,\mathrm{g\,cm^{-3}}$ (red) for models B0 (left), B15-nl (center left), model B15-low (center right), and B15-high (right). The rednerings depict the simulations towards the end of the steady outflow rate phase at $t - t_{\mathrm{map}} = 15.1\,\mathrm{ms}$ for B15-nl, at $t - t_{\mathrm{map}} = 19.4\,\mathrm{ms}$ for B0 and B15-low, and at $t - t_{\mathrm{map}} = 20.9\,\mathrm{ms}$ for B15-high. The different times reflect the different collapse

[Mosta+ 2020]

They see jet formation from the remnant (before the collapse) only if strong large-scale field and neutrinos are included

Merging Neutron Stars

Most works for simplicity start with magnetar-like values of purely dipolar fields (10^{15} G), either in the pre-merger or directly in the post-merger stage.

What are the typical magnetic fields expected for merging neutron stars?

Typically, we expect NSs to merge at Gyr ages or later.

[Farrow+ 2019]

Pulsar Name	M_T ($M_\odot$)	m_r ($M_\odot$)	m_s ($M_\odot$)	$\mathcal{M}_c$ ($M_\odot$)	q	P_b (day)	T_c (Gyr)	References
Systems will merge within a Hubble time								
J1946+2052	2.50(4)	< 1.35	> 1.17	(1.05, 1.11)	(0.68, 1)	0.078	0.046	(1)
J1756−2251	2.56999(6)	1.341(7)	1.230(7)	1.1178(3)	0.92(1)	0.320	1.656	(2)
J0737−3039A/B	2.58708(16)	1.3381(7)	1.2489(7)	1.1253(1)	0.933(1)	0.102	0.086	(3)
J1906+0746	2.6134(3)	1.322(11)	1.291(11)	1.1372(2)	(0.956, 1)	0.166	0.308	(4)
B1534+12	2.678463(4)	1.3330(2)	1.3455(2)	1.165870(2)	0.9907(3)	0.421	2.734	(5)
B2127+11C	2.71279(13)	1.358(10)	1.354(10)	1.18043(8)	(0.975, 1)	0.335	0.217	(6)
J1757−1854	2.73295(9)	1.3384(9)	1.3946(9)	1.18930(4)	0.960(1)	0.184	0.076	(7)
J0509+3801	2.805(3)	1.34(8)	1.46(8)	1.215(5)	(0.793, 1)	0.380	0.574	(8)
B1913+16	2.828378(7)	1.4398(2)	1.3886(2)	1.230891(5)	0.9644(3)	0.323	0.301	(9)
J1913+1102	2.886(1)	1.65(5)	1.24(5)	1.242(8)	0.75(5)	0.206	0.473	(10)
Systems will not merge within a Hubble time								
J1807−2500B	2.57190(73)	1.3655(21)	1.2064(21)	1.1169(3)	0.883(3)	9.957	1044	(11)
J1518+4904	2.7183(7)	1.41(8)	1.31(8)	1.181(5)	(0.794, 1)	8.634	8832	(12)
J0453+1559	2.733(4)	1.559(5)	1.174(4)	1.175(2)	0.753(5)	4.072	1453	(13)
J1411+2551	2.538(22)	< 1.64	> 0.92	(1.05, 1.11)	(0.57, 0.95)	2.616	466	(14)
J1811−1736	2.57(10)	< 1.75	> 0.91	(1.02, 1.17)	(0.58, 0.95)	18.78	1794	(15)
J1829+2456	2.59(2)	< 1.36	> 1.25	(1.08, 1.14)	(0.65, 1)	1.176	55	(16)
J1930−1852	2.59(4)	< 1.32	> 1.30	(1.07, 1.15)	(0.58, 0.96)	45.06	$\sim 10^5$	(17)

Table 1. Mass measurements of Galactic DNS systems: the binary total mass (M_T), the masses of the recycled NS (m_r) and the slow NS (m_s), binary chirp mass ($\mathcal{M}_c$), mass ratio (q), binary orbital period (P_b) and coalescence time T_c. Figures

Isolated Neutron Stars: magnetic field decay

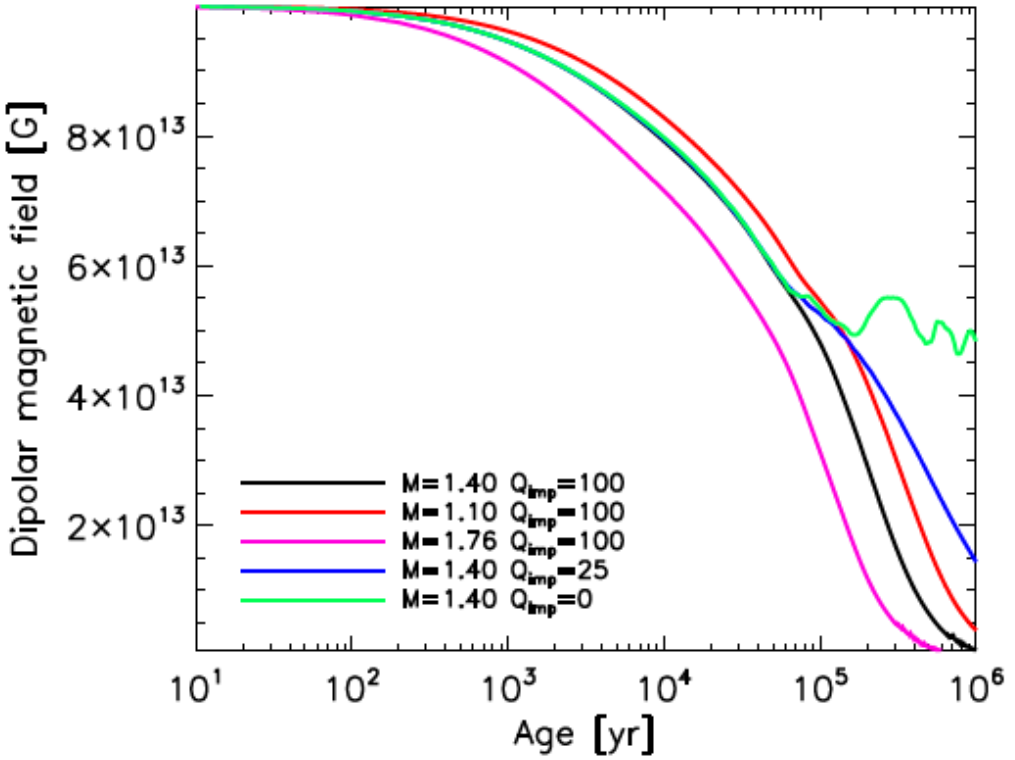

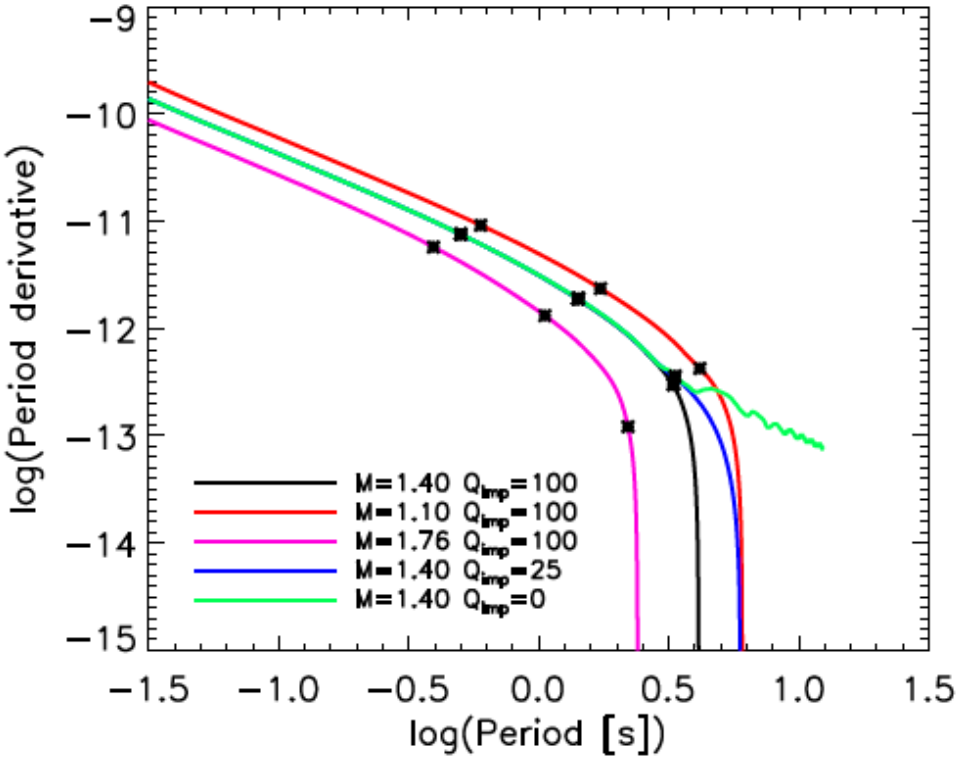

[Viganò+ 2013]

Strong magnetic fields decay on Myr timescales (or less) due to crustal resistivity.

Old isolated Neutron Stars

Old isolated pulsars difficult to be detected: radio-luminosity fades for high periods and low Pdot (i.e., low B since it decayed).

Millisecond pulsars are recycled (low P and Pdot): typically, 10^8-10^9 G.
100 pulsars with only upper limits on B, down to less than 10^8 G.

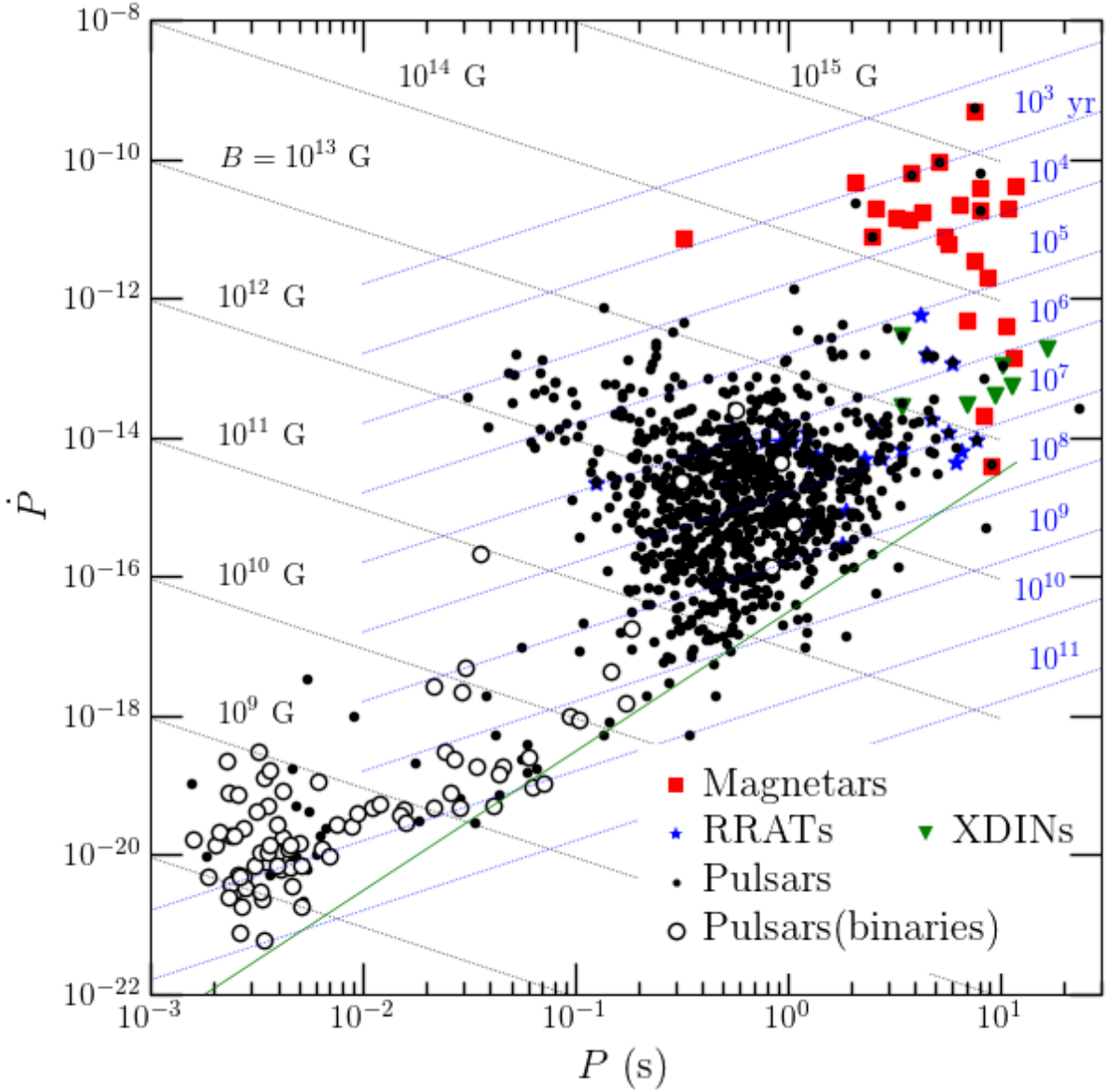

[A. W. Steiner www.neutronstars.utk.edu]

"Recycling" old Neutron Stars

1. Main-sequence star + Evolved massive star

2. Evolved star explodes leaving a neutron star

3. The main-sequence star evolves to giant and triggers accretion onto the neutron star, speeding up its rotation and making it X-ray bright

4. The neutron star becomes visible as millisecond pulsar and erodes away the companion

[Alpar 1982]

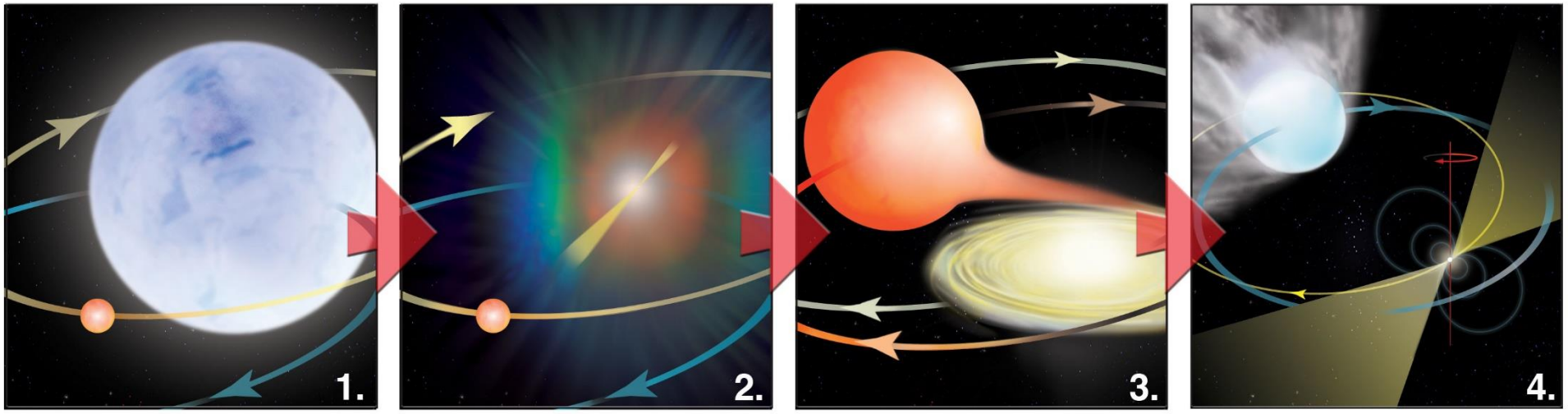

[Scott Ransom NRAO]

Old Neutron Stars in low-mass X-ray binaries

Old compact object (NS or BH) + low-mass companion (several subclasses).

Accretion by Roche lobe overflow:
X-ray bright disk + sporadic thermonuclear bursts.

No direct measurement of magnetic fields (for instance, no cyclotron lines in the spectra): only model-dependent estimates related to quasi-periodic oscillations or magnetospheric radius. Typically, upper limit 10^8-10^9 G

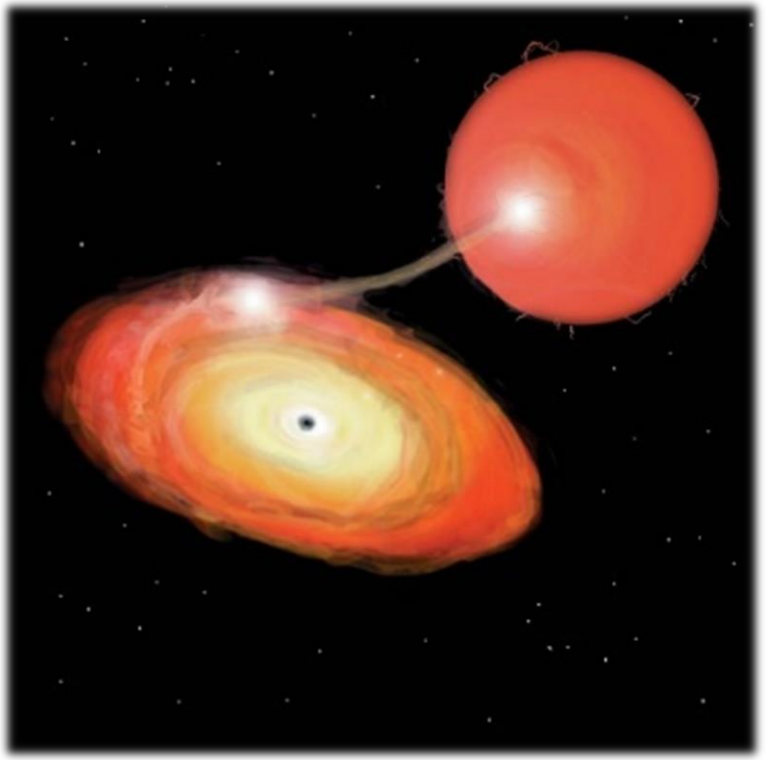

Old Neutron Stars

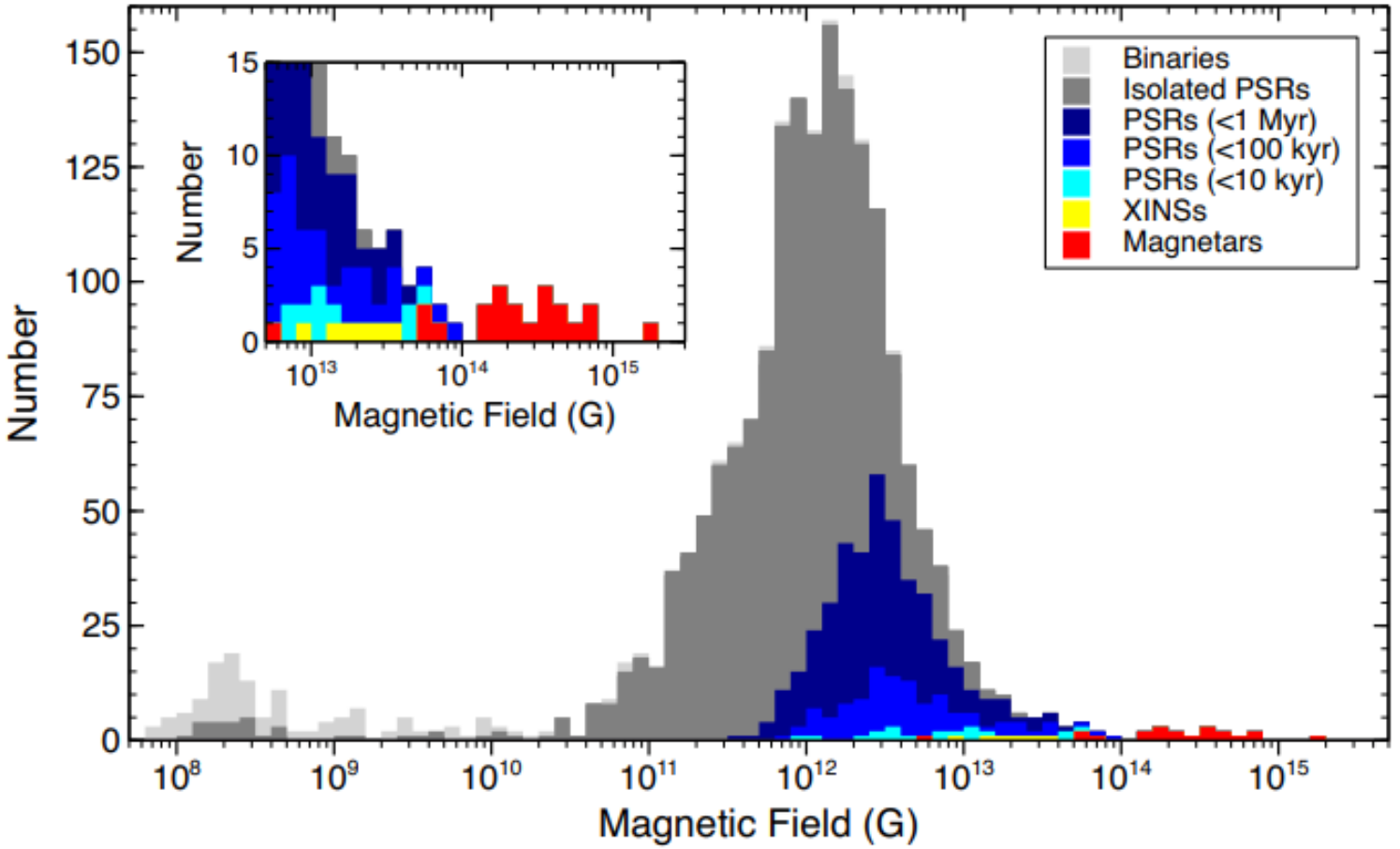

[Olausen & Kaspi 2014]

Any choice of Gyr-old NS with B >> 10^9 G is unsupported.

Topology: behind the dipole

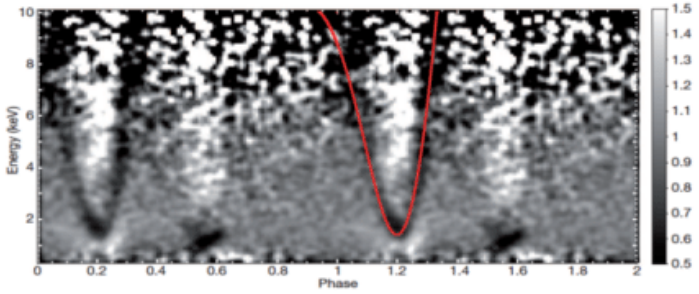

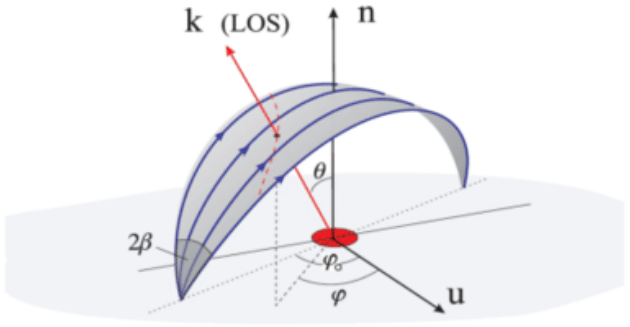

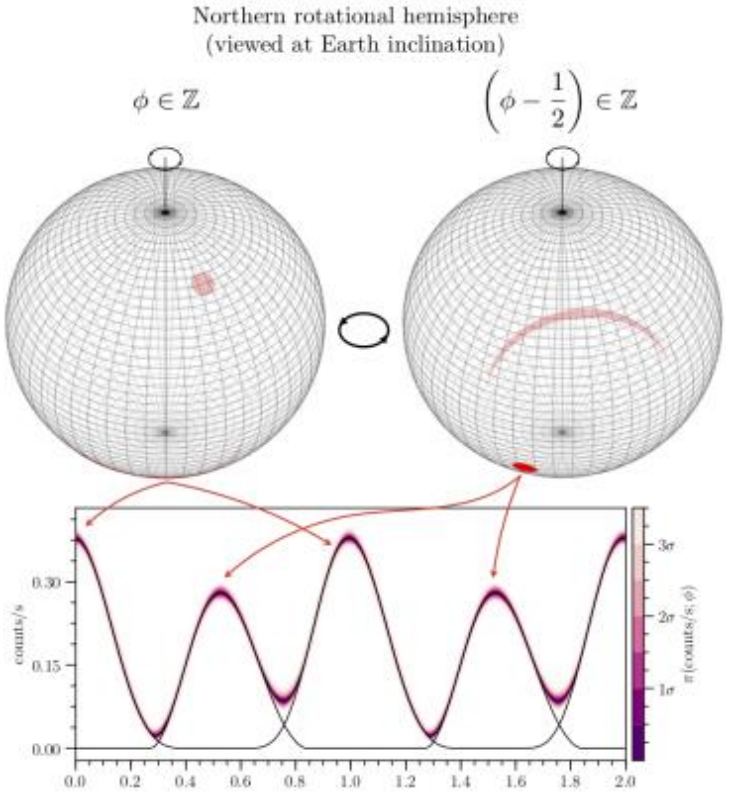

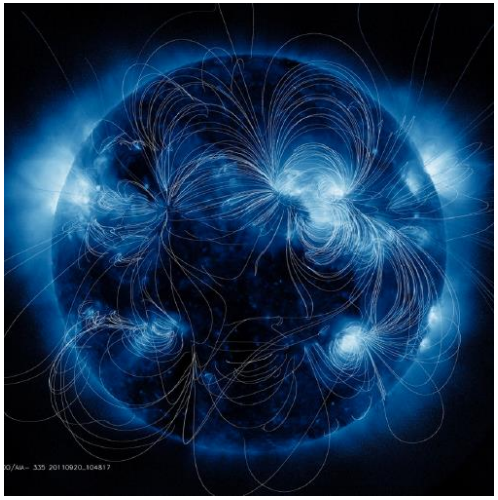

Hints for non-dipolarity in several neutron stars (young and old) inferred from X-rays spectra and light curves

Magnetic field amplification: MHD

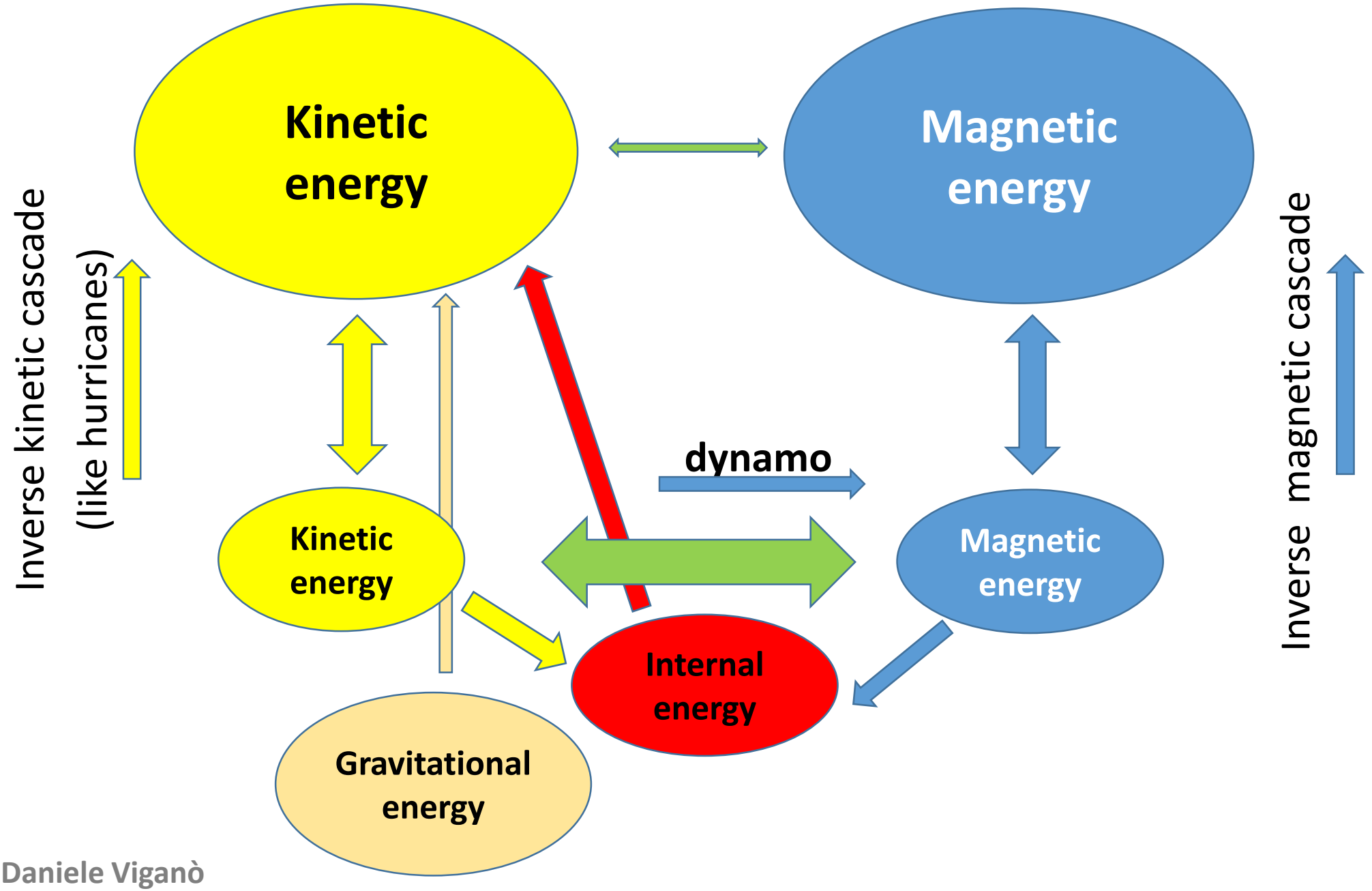

Simulating large eddies, modeling small eddies

Widely used in plasma physics, engineering (incompressible), solar physics.

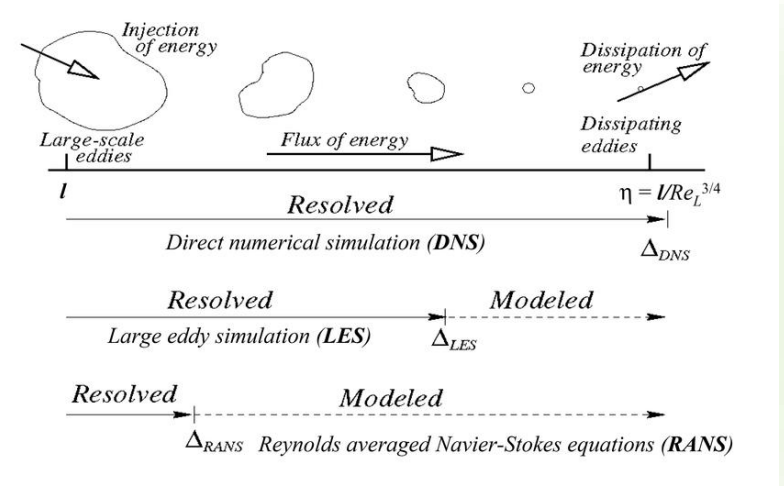

[Foroozani 2015]

Finite resolution corresponds to an effective spatial filter for the variables:

$$f(\vec{x},t) = \overline{f}(\vec{x},t) + f'(\vec{x},t)$$

Models can be explicit (Sub-Grid Scale/residual-based models), or implicitly given by the numerical dissipation (implicit LES, non-controllable and intrinsic to the scheme used)

The simplest example

Take the simplest non-linear evolution equation, Burgers:

$$\partial_t u + \frac{1}{2}\partial_x u^2 = 0$$

Apply the filter and **express your discretized equations only in terms of the resolved evolved fields:**

$$\partial_t \bar{u} + \frac{1}{2}\partial_x \bar{u}^2 = \partial_x \bar{\tau}, \qquad \bar{\tau} \equiv \bar{u}^2 - \overline{u^2}$$

The new sub-filter-scale tensor is not known, by definition.
It needs to be modelled (or ignored)

Further example: compressible non-relativistic MHD *[Viganò+ 2019]*

$$\partial_t(\overline{\rho}\tilde{v}^i) + \partial_k\left[\overline{\rho}\tilde{v}^k\tilde{v}^i - \overline{B}^k\overline{B}^i + \delta^{ki}\left\{p(\overline{\rho},\tilde{e}) + \frac{1}{2}\overline{B}^2\right\}\right] =$$

$$= \partial_k\left[\overline{\tau}^{ki}_{\rm kin} - \overline{\tau}^{ki}_{\rm mag} + \delta^{ki}\delta_{lm}\left(\overline{\tau}^{lm}_{\rm p} + \frac{1}{2}\overline{\tau}^{lm}_{\rm mag}\right)\right] \quad (13)$$

$$\partial_t\overline{B}^i + \partial_k\left[\tilde{v}^k\overline{B}^i - \tilde{v}^i\overline{B}^k\right] = \partial_k\overline{\tau}^{ki}_{\rm ind} \quad (14)$$

$$\partial_t\overline{U} + \partial_k\left[\widetilde{\Theta}\,\tilde{v}^k - (\tilde{v}_j\overline{B}^j)\overline{B}^k\right] = \partial_k[\overline{\tau}^k_{\rm adv} - \overline{\tau}^k_{\rm hel}]$$

$$\widetilde{\Theta} = \overline{U} + \tilde{p} + \frac{\overline{B}^2}{2}$$

$$\overline{\tau}^{ki}_{\rm kin} = \overline{\rho}\,\tilde{v}^k\,\tilde{v}^i - \overline{\rho v^k v^i}$$

$$\overline{\tau}^{ki}_{\rm mag} = \overline{B}^k\,\overline{B}^i - \overline{B^k B^i}$$

$$\overline{\tau}^{ki}_{\rm ind} = (\tilde{v}^k\,\overline{B}^i - \tilde{v}^i\,\overline{B}^k) - (\overline{v^k B^i} - \overline{v^i B^k})$$

$$\overline{\tau}_{\rm pres} = \tilde{p} - \overline{p} + \frac{1}{2}\overline{\tau}^{jm}_{\rm mag}\delta_{jm}$$

$$\overline{\tau}^k_{\rm adv} = \widetilde{\Theta}\,\tilde{v}^k - \overline{\Theta v^k}$$

$$\overline{\tau}^k_{\rm hel} = (\tilde{v}_j\,\overline{B}^j)\,\overline{B}^k - \overline{(v_j B^j)B^k}$$

Discretization (i.e., filtering) makes you lose some information contained in the Sub-Filter Scales, in the non-linear terms of the fluxes.

How to model them as a function of the known filtered values?

Assessment tools: a-priori test

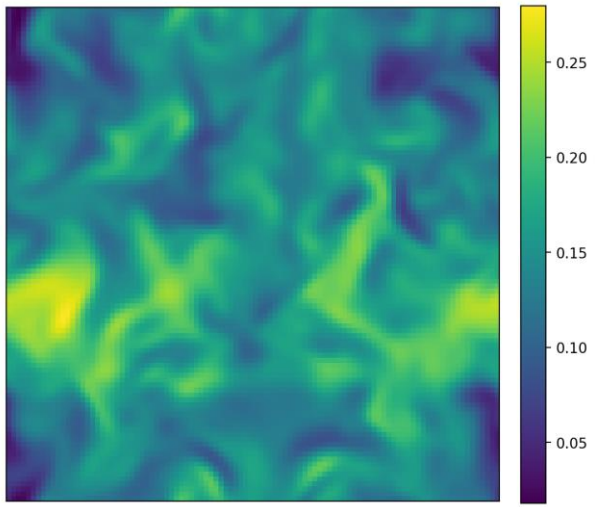

Original resolution

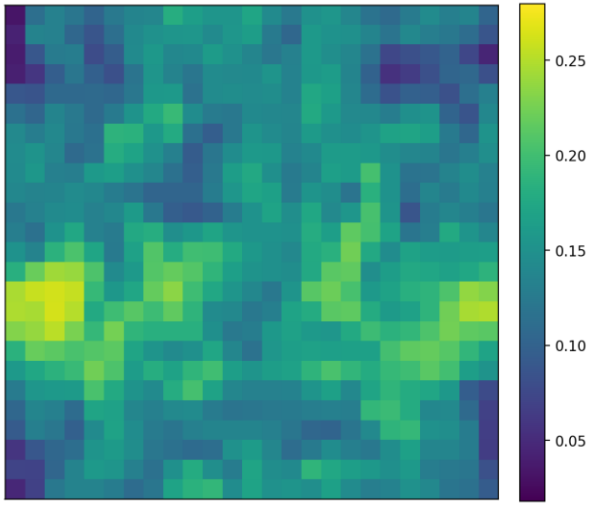

Filtered resolution

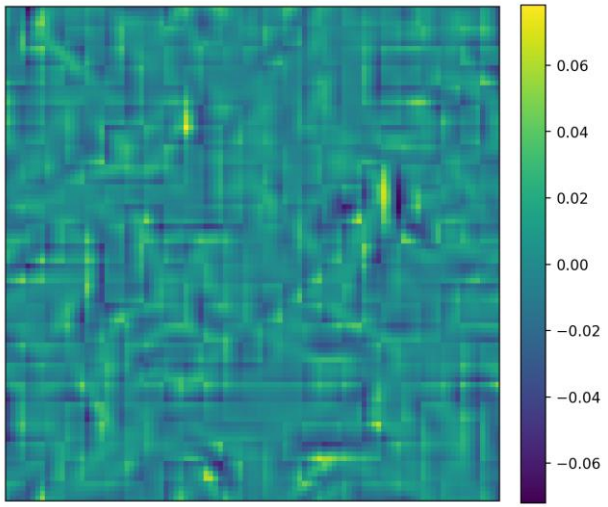

Sub-Filter Scale loss

1. Take a snapshot of a simulation and calculate the information loss for an original resolution and filter (right image)
2. Calculate your SGS model applied to the filtered fields (center image).
3. Look the correlation between SGS and SFS (N^3 points) and find the best-fit pre-coefficient $C_{best}^{ki} = \frac{\Sigma\, \overline{\tau}^{ki}(\vec{x})\, \tau^{ki}(\vec{x})}{\Sigma\, \tau^{ki}(\vec{x})^2}$
4. Repeat for different time, resolutions, filter size, initial conditions, times… Ideally, you want a constant best-fit coefficient and a high Pearson value

Sub-grid-scale modeling: dissipative

Turbulent viscosity term in the momentum equation (prop. to strain rate) and turbulent resistive term (prop. to current) in the induction equation.

$$\overline{\tau}^{ki}_{\rm kin} = \Delta^2 \overline{\rho} |\tilde{S}| \tilde{S}^{ki}$$

$$\tau^{ki}_{\rm ind} = \Delta^2 \frac{|\overline{J}|}{\sqrt{\overline{\rho}}} \overline{J}^{ki}$$

Applied also in GRHD mergers [Radice 2017-2020, Shibata & Kouichi 2017]:

$$\tau_{ij} = -2\nu_T (e+p) W^2 \left[\frac{1}{2}\left(D_i \overline{v}_j + D_j \overline{v}_i \right) - \frac{1}{3} D_k \overline{v^k} \gamma_{ij} \right] , \qquad \nu_T = \ell_{\rm mix}\, c_s \,, \quad \ell_{\rm mix} = \alpha\, c_s\, \Omega^{-1} \,,$$

where l_{mix} is calibrated by high-resolution simulations.

It **only allows transfer from large to small scales**. It can simulate the effective viscous magnetic force but not inverse (non-local) cascades.

Sub-grid-scale modeling in mergers: dynamo-like

[Palenzuela 2015+] vorticity-dependent dynamo term in the ideal MHD induction equation

$$\partial_t(\sqrt{\gamma}B^i) = \cdots + \alpha\sqrt{\gamma}\xi B^i.$$

Here we have defined the amplification factor as

$$\xi \equiv \xi_0\Theta(\rho[\omega^z - \omega^z_{\rm thresh}])g(t)B_k v^k,$$

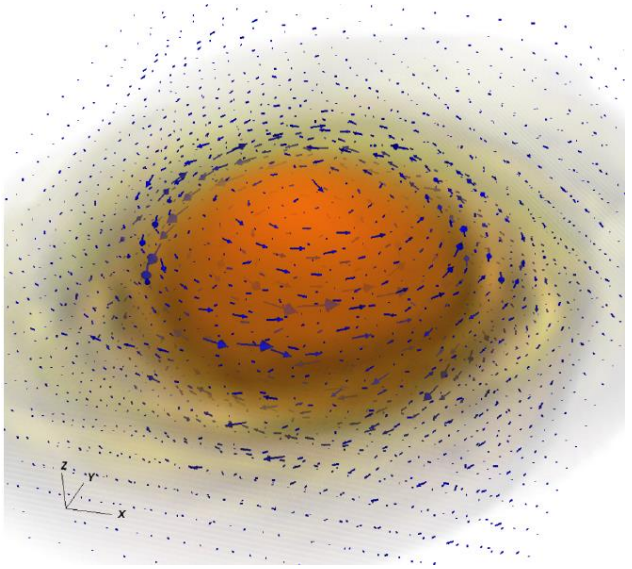

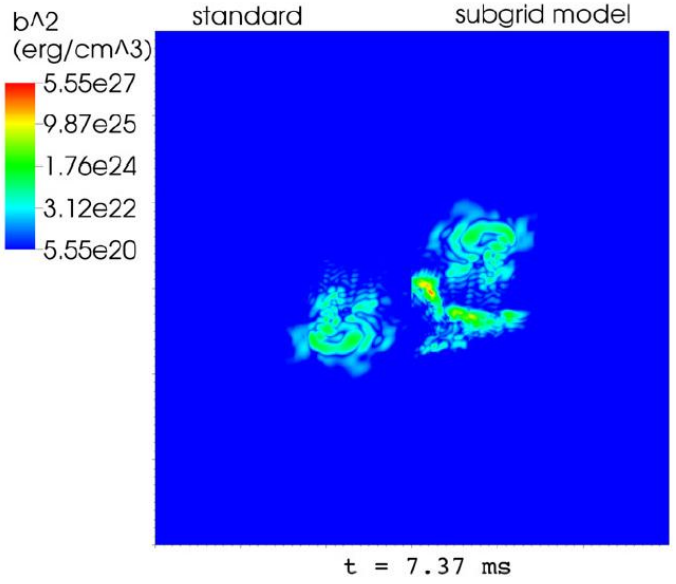

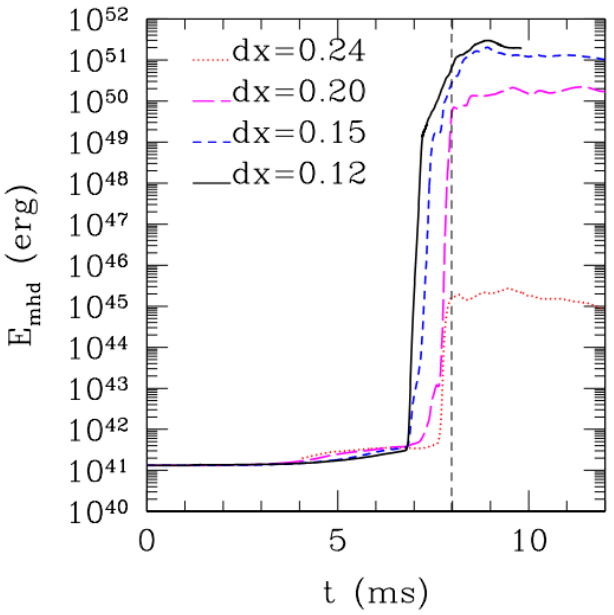

[Giacomazzo 2015+]

$$\vec{E}_{\rm subgrid} = -S_{\rm subgrid}\vec{A}$$

$$S_{\rm subgrid} \equiv c_1 \max\left(|\nabla \times v| - c_3, 0\right) \times \max\left(1 - c_4\frac{\rho_{\rm atmo}}{\rho}, 0\right) \times \max\left(1 - \frac{b^2}{c_2\Delta w}, 0\right),$$

Sub-grid-scale modeling: gradient model

The finite resolution can be thought as a filter of conserved equations:

$$\partial_t \bar{U}^a + \partial_k F^{ka}(\bar{U}) = \partial_k \bar{\tau}^{ka},$$

$$\bar{\tau}_F^{ka} := F^{ka}(\bar{U}) - \overline{F^{ka}(U)}.$$

For mathematical convenience, let's assume a Gaussian kernel

$$\bar{f}(\mathbf{x},t) = \int_{-\infty}^{\infty} G(\mathbf{x}-\mathbf{x}') f(\mathbf{x}',t) d^3x'. \qquad G_i(|x_i - x_i'|) = \left(\frac{1}{4\pi\xi}\right)^{1/2} \exp\left(\frac{-|x_i - x_i'|^2}{4\xi}\right),$$

Its inverse Fourier transform, expanded in series of xi, is:

$$\frac{1}{\hat{G}(\mathbf{k})} = \sum_{n=0}^{\infty} \frac{1}{n!} (\xi \mathbf{k}^2)^n. \qquad f \equiv G^{-1} * \bar{f} = \sum_{n=0}^{\infty} \frac{(-1)^n}{n!} (\xi \nabla^2)^n \bar{f}.$$

Sub-grid-scale modeling: gradient model

The first-order Taylor expansion of the deconvolution of a Gaussian filter in the Fourier space: recipe for any non-linear terms. For a generic filtered product, we can **approximate its unknown filtered value with the filtered fields and their gradients (that we know)**:

$$\overline{fg} \backsimeq \overline{f}\,\overline{g} + 2\,\xi\,\nabla\overline{f}\cdot\nabla\overline{g}$$

$$\overline{f(g)} \backsimeq f(\bar{g}) + \xi\left(\nabla^2 f(\bar{g}) - \frac{df}{d\bar{g}}\nabla^2\bar{g}\right)$$

$$\backsimeq f(\bar{g}) + \xi\nabla\frac{df}{d\bar{g}}\cdot\nabla\bar{g},$$

$$\xi = \Delta^2/24$$

The new terms vanish by construction in the continuous limit (as most SGS models do).

Sub-grid-scale modeling: gradient model

Consider evolution equations with fluxes and conserved variables as a function of primitive variables P

$$\partial_t \bar{C}^a + \partial_k F^{ka}(\tilde{P}) = \partial_k \bar{\tau}^{ka}, \qquad C^a = f^a(P), \qquad P^a := (f^{-1})^a(C) \equiv g^a(C).$$
$$\tilde{P}^a := g^a(\bar{C})$$

The SFS residuals are

$$\bar{\tau}_F^{ka} := F^{ka}(\tilde{P}) - \overline{F^{ka}(P)},$$

and can be modelled by alternative formulations:

$$\tau_F^{ka} = \xi\left(\frac{dF^{ka}}{d\tilde{P}^b}\frac{d\tilde{P}^b}{d\bar{C}^e}\nabla^2\bar{C}^e - \nabla^2 F^{ka}(\tilde{P})\right),$$

$$\tau_F^{ka} = -\xi\nabla\frac{dF^{ka}}{d\bar{C}^b}\cdot\nabla\bar{C}^b.$$

Depending on the non-linear form in fluxes, expressions can be cumbersome

Gradient model for compressible MHD [Viganò+ 2019]

DISCRETIZED EQUATIONS

$$\partial_t(\overline{\rho}\tilde{v}^i) + \partial_k\left[\overline{\rho}\tilde{v}^k\tilde{v}^i - \overline{B}^k\overline{B}^i + \delta^{ki}\left\{p(\overline{\rho},\tilde{e}) + \frac{1}{2}\overline{B}^2\right\}\right] =$$

$$= \partial_k\left[\overline{\tau}^{ki}_{\rm kin} - \overline{\tau}^{ki}_{\rm mag} + \delta^{ki}\delta_{lm}\left(\overline{\tau}^{lm}_{\rm p} + \frac{1}{2}\overline{\tau}^{lm}_{\rm mag}\right)\right] \quad (13)$$

$$\partial_t\overline{B}^i + \partial_k\left[\tilde{v}^k\overline{B}^i - \tilde{v}^i\overline{B}^k\right] = \partial_k\overline{\tau}^{ki}_{\rm ind} \quad (14)$$

$$\partial_t\overline{U} + \partial_k\left[\widetilde{\Theta}\,\tilde{v}^k - (\tilde{v}_j\overline{B}^j)\overline{B}^k\right] = \partial_k[\overline{\tau}^k_{\rm adv} - \overline{\tau}^k_{\rm hel}]$$

UNKNOWN SFS TERMS

$$\overline{\tau}^{ki}_{\rm kin} = \overline{\rho}\,\tilde{v}^k\,\tilde{v}^i - \overline{\rho v^k v^i}$$

$$\overline{\tau}^{ki}_{\rm mag} = \overline{B}^k\,\overline{B}^i - \overline{B^k B^i}$$

$$\overline{\tau}^{ki}_{\rm ind} = (\tilde{v}^k\,\overline{B}^i - \tilde{v}^i\,\overline{B}^k) - (\overline{v^k B^i} - \overline{v^i B^k})$$

$$\overline{\tau}_{\rm pres} = \widetilde{p} - \overline{p} + \frac{1}{2}\overline{\tau}^{jm}_{\rm mag}\delta_{jm}$$

$$\overline{\tau}^k_{\rm adv} = \widetilde{\Theta}\,\tilde{v}^k - \overline{\Theta v^k}$$

$$\overline{\tau}^k_{\rm hel} = (\tilde{v}_j\,\overline{B}^j)\,\overline{B}^k - \overline{(v_j B^j)B^k}$$

GRADIENT SGS MODEL TERMS

$$\tau^{ki}_{\rm kin} = -2\xi\,\overline{\rho}\,\partial_j\tilde{v}^k\,\partial^j\tilde{v}^i$$

$$\tau^{ki}_{\rm mag} = -2\xi\,\partial_j\overline{B}^k\,\partial^j\overline{B}^i$$

$$\tau^{ki}_{\rm ind} = -2\xi\left[\partial_j\tilde{v}^k\left(\partial^j\overline{B}^i - \frac{\overline{B}^i}{\overline{\rho}}\partial^j\overline{\rho}\right) - \partial_j\tilde{v}^i\left(\partial^j\overline{B}^k - \frac{\overline{B}^k}{\overline{\rho}}\partial^j\overline{\rho}\right)\right].$$

$$\tau^k_{\rm adv} = \tau_{\rm pres}\tilde{v}^k - 2\xi\left(\partial_j\widetilde{\Theta}\partial^j\tilde{v}^k - \frac{\Theta}{\overline{\rho}}\partial_j\overline{\rho}\partial^j\tilde{v}^k\right)$$

$$\tau^k_{\rm hel} = -2\xi\left[\partial_j(\tilde{v}_m\overline{B}^m)\partial^j\overline{B}^k + \overline{B}^k\partial^j\tilde{v}^m\left(\partial_j\overline{B}_m - \frac{\overline{B}_m}{\overline{\rho}}\partial_j\overline{\rho}\right)\right]$$

Assessment with KHI box simulations *[Viganò+ 2019]*

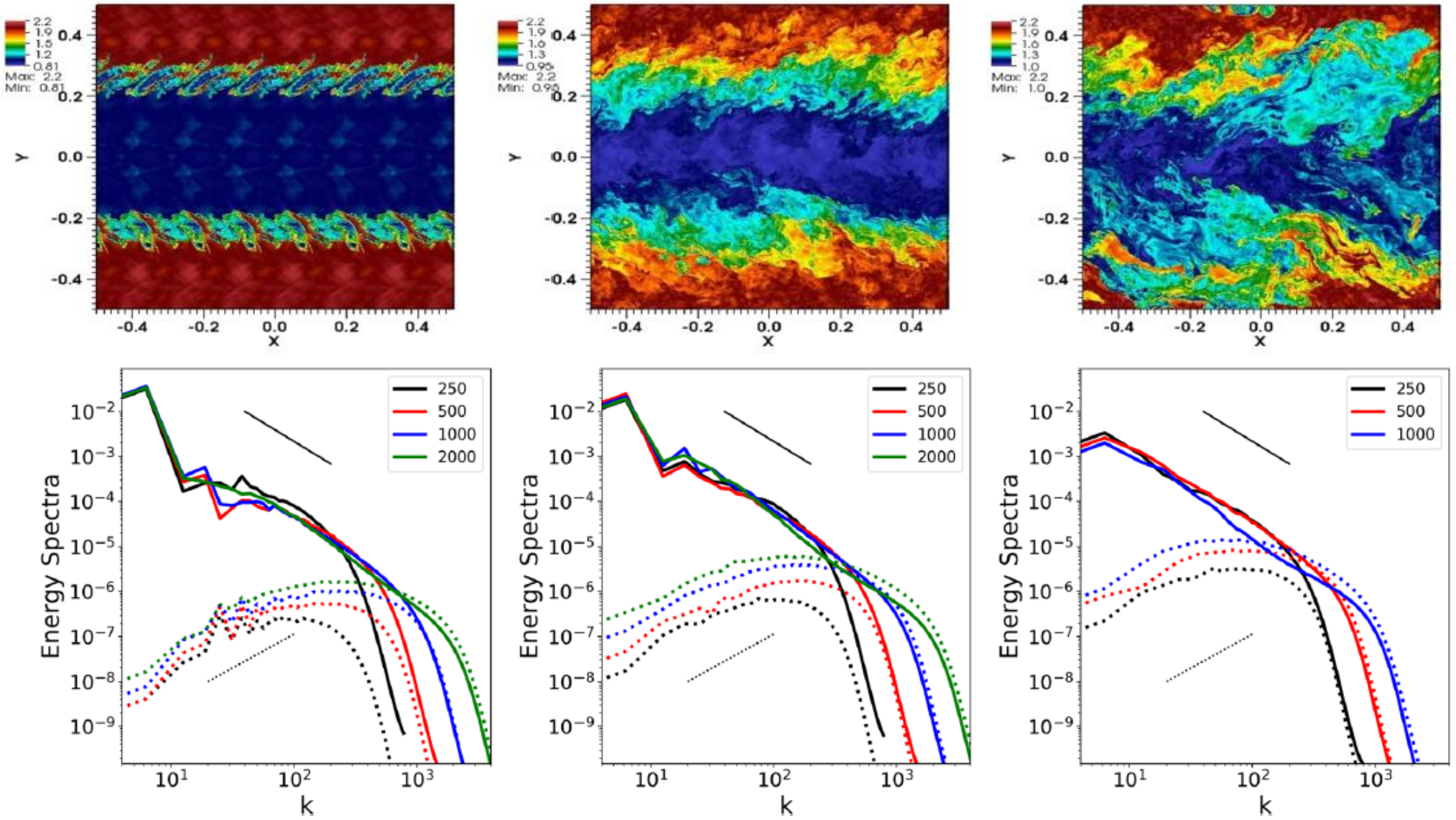

Compressible MHD: a-priori test for different SGS models

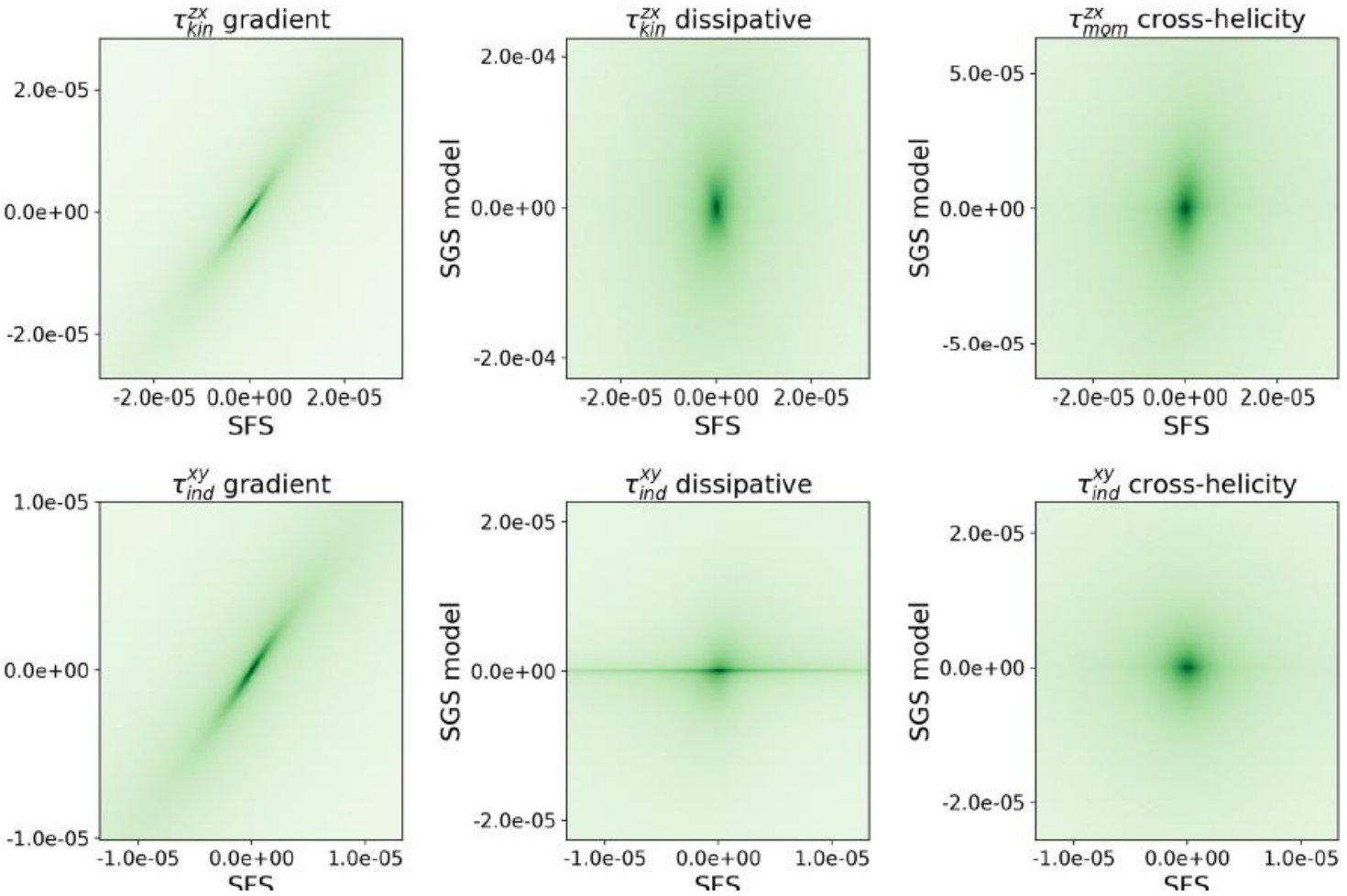

Gradient model outperforms the other models tested for all:

- Tensor components
- Resolutions
- Filter sizes
- Initial conditions
- Times

[Viganò+ 2019]

See also Machine Learning SGS models applied to the same problem in 2D can perform better [Rosofsky & Huerta 2020] (but how costly is to train them?)

Compressible MHD: a-posteriori test *[Viganò+ 2019]*

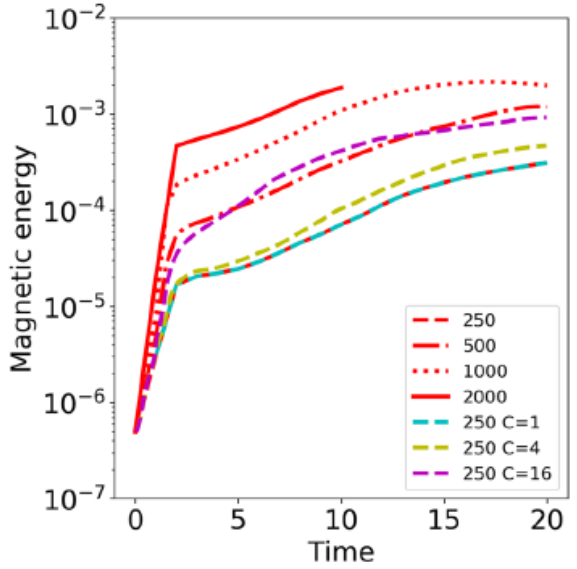

Compare high resolution runs with low resolution + SGS.

Need for large values of the free parameter C. Probably due to the numerical dissipation of the scheme.

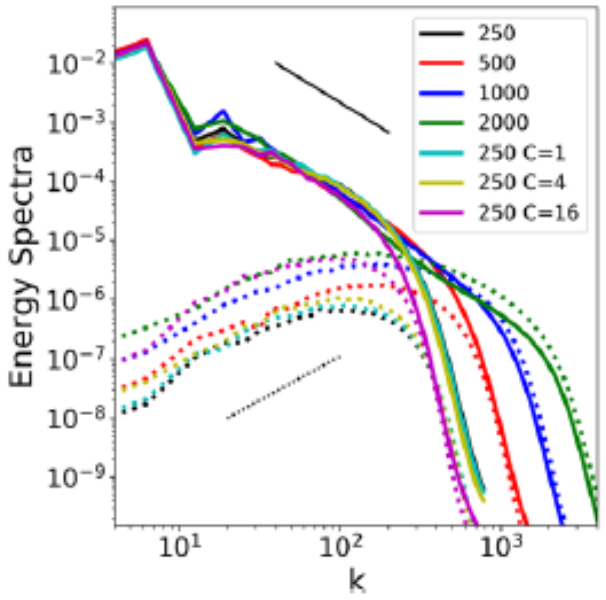

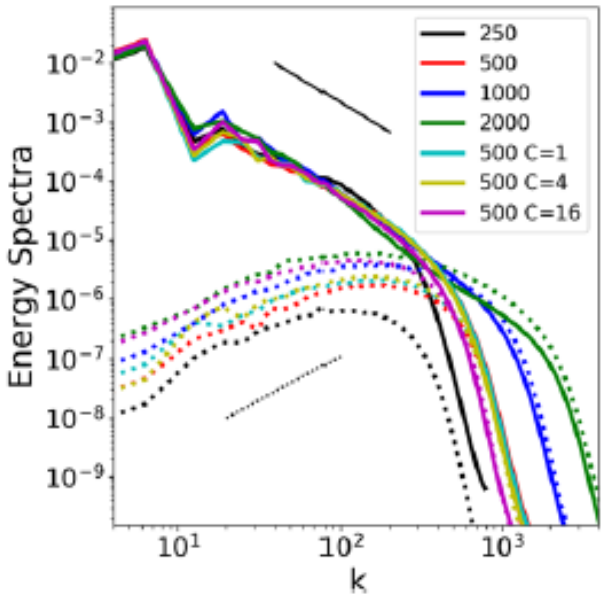

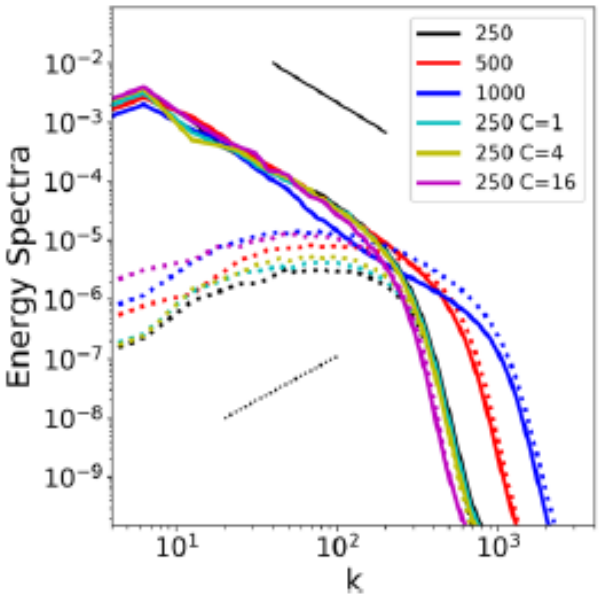

Gradient model for special relativistic MHD [Carrasco+ 2020]

$$\partial_t D + \partial_k N^k = 0, \qquad N^k = D v^k,$$

$$\partial_t S^i + \partial_k T^{ki} = 0,$$

$$\partial_t U + \partial_k S^k = 0,$$

$$\partial_t B^i + \partial_k M^{ki} = 0, \qquad M^{ki} = 2B^{[i} v^{k]},$$

$$T^{ki} = hW^2 v^k v^i - E^k E^i - B^k B^i + \delta^{ki}\left[p + \frac{1}{2}(E^2 + B^2)\right]$$

$$D = \rho W,$$

$$S^i = (hW^2 + B^2)v^i - (v \cdot B)B^i,$$

$$U = hW^2 - p + B^2 - \frac{1}{2}\left[(v \cdot B)^2 + \frac{B^2}{W^2}\right],$$

Filtered (discretized + SGS terms):

$$\partial_t \bar{D} + \partial_k N^k(\tilde{P}) = \partial_k \bar{\tau}_N^k,$$

$$\partial_t \bar{S}^i + \partial_k T^{ki}(\tilde{P}) = \partial_k \bar{\tau}_T^{ki},$$

$$\partial_t \bar{U} + \partial_k S^k(\tilde{P}) = \partial_k \bar{\tau}_S^k,$$

$$\partial_t \bar{B}^i + \partial_k M^{ki}(\tilde{P}) = \partial_k \bar{\tau}_M^{ki},$$

$$\tau_N^k = -\xi H_N^k, \qquad \tau_T^{ki} = -\xi H_T^{ki}$$

$$\tau_S^k = 0, \qquad \tau_M^{ki} = -\xi H_M^{ki},$$

$$H_N^k = 2\nabla \bar{D} \cdot \nabla \tilde{v}^k + \bar{D} H_v^k, \tag{48}$$

$$\begin{aligned} H_T^{ki} = {} & 2[\nabla \tilde{\mathcal{E}} \cdot \nabla(\tilde{v}^i \tilde{v}^k) + \tilde{\mathcal{E}}(\tilde{v}^{(i} H_v^{k)} + \nabla \tilde{v}^i \cdot \nabla \tilde{v}^k)] \\ & + \tilde{v}^i \tilde{v}^k H_{\mathcal{E}} - 2[\nabla \bar{B}^i \cdot \nabla \bar{B}^k + \nabla \tilde{E}^i \cdot \nabla \tilde{E}^k + \tilde{E}^{(i} H_E^{k)}] \\ & + \delta^{ki}[H_p + \nabla \bar{B}_j \cdot \nabla \bar{B}^j + \nabla \tilde{E}_j \cdot \nabla \tilde{E}^j + \tilde{E}_j H_E^j], \end{aligned} \tag{49}$$

$$H_M^{ki} = 4\nabla \bar{B}^{[i} \cdot \nabla \tilde{v}^{k]} + 2\bar{B}^{[i} H_v^{k]}, \tag{50}$$

Gradient model for special relativistic MHD

[Carrasco+ 2020]

$$\tilde{\Psi}_v^k = \frac{2}{\tilde{\Theta}}\left\{\nabla(\tilde{v}\cdot\bar{B})\cdot\nabla\bar{B}^k - \nabla\tilde{\Theta}\cdot\nabla\tilde{v}^k + \frac{\bar{B}^k}{\tilde{\mathcal{E}}}[\tilde{\Theta}\nabla\bar{B}_j\cdot\nabla\tilde{v}^j + \bar{B}_j\nabla\bar{B}^j\cdot\nabla(\tilde{v}\cdot\bar{B}) - \bar{B}_j\nabla\tilde{v}^j\cdot\nabla\tilde{\Theta}]\right\},$$

$$\tilde{\Psi}_M^{ki} = \frac{4}{\tilde{\Theta}}[\tilde{\Theta}\nabla\bar{B}^{[i}\cdot\nabla\tilde{v}^{k]} + \bar{B}^{[i}\nabla\bar{B}^{k]}\cdot\nabla(\tilde{v}\cdot\bar{B}) - \bar{B}^{[i}\nabla\tilde{v}^{k]}\cdot\nabla\tilde{\Theta}],$$

$$\tilde{\Psi}_\Theta = \frac{\tilde{\Theta}}{\tilde{\Theta}-\tilde{E}^2}\{\nabla\bar{B}_j\cdot\nabla\bar{B}^j - \nabla\tilde{E}_j\cdot\nabla\tilde{E}^j - \bar{B}_{[i}\tilde{v}_{k]}\tilde{\Psi}_M^{ki}\},$$

$$\tilde{\Psi}_A = \tilde{W}^2\left(\tilde{p}\frac{d\tilde{p}}{d\tilde{\epsilon}} + \tilde{\rho}^2\frac{d\tilde{p}}{d\tilde{\rho}}\right),$$

$$\begin{aligned}\frac{H_{\mathrm{p}}}{\tilde{\Theta}-\tilde{E}^2} = {}& \frac{\tilde{\mathcal{E}}\tilde{W}^2}{(\tilde{\rho}\,\tilde{\mathcal{E}}-\tilde{\Psi}_A)(\tilde{\Theta}-\tilde{E}^2)\tilde{W}^2 + \tilde{\Psi}_A\tilde{\Theta}}\left\{\tilde{\rho}\left(\nabla\frac{d\tilde{p}}{d\tilde{\rho}}\cdot\nabla\tilde{\rho} + \nabla\frac{d\tilde{p}}{d\tilde{\epsilon}}\cdot\nabla\tilde{\epsilon}\right) - 2\frac{d\tilde{p}}{d\tilde{\epsilon}}\nabla\tilde{\rho}\cdot\nabla\tilde{\epsilon}\right.\\ & - \left(\tilde{\mathcal{E}}\frac{d\tilde{p}}{d\tilde{\epsilon}} - \tilde{\Psi}_A\right)\left[\frac{\tilde{W}^2}{4}\nabla\tilde{W}^{-2}\cdot\nabla\tilde{W}^{-2} + \nabla\tilde{W}^{-2}\cdot\nabla(\ln\tilde{\rho})\right] - \frac{2}{\tilde{W}^2}\frac{d\tilde{p}}{d\tilde{\epsilon}}[\nabla\bar{B}_j\cdot\nabla\bar{B}^j + \nabla\tilde{W}^2\cdot\nabla\tilde{h}]\\ & \left. - \left(\tilde{\mathcal{E}}\frac{d\tilde{p}}{d\tilde{\epsilon}} + \tilde{\Psi}_A\right)[\tilde{v}_k\tilde{\Psi}_v^k + \nabla\tilde{v}_j\cdot\nabla\tilde{v}^j + \tilde{W}^2\nabla\tilde{W}^{-2}\cdot\nabla\tilde{W}^{-2}] + \frac{1}{\tilde{\mathcal{E}}}\left[\left(\tilde{\mathcal{E}}\frac{d\tilde{p}}{d\tilde{\epsilon}} + \tilde{\Psi}_A\right)(\tilde{\Theta}-\tilde{E}^2) - \frac{\tilde{\Psi}_A\tilde{\Theta}}{\tilde{W}^2}\right]\frac{\tilde{\Psi}_\Theta}{\tilde{\Theta}}\right\},\end{aligned}$$

$$H_{\mathcal{E}} = H_p - \nabla\bar{B}_j\cdot\nabla\bar{B}^j - \nabla\tilde{E}_j\cdot\nabla\tilde{E}^j - \tilde{E}_k H_E^k,$$

$$H_\Theta = \tilde{\Psi}_\Theta + \frac{\tilde{\Theta}}{\tilde{\Theta}-\tilde{E}^2}H_p,$$

$$H_v^k := \tilde{\Psi}_v^k - \left(\tilde{v}^k + \frac{\tilde{v}\cdot\bar{B}}{\tilde{\mathcal{E}}}\bar{B}^k\right)\frac{H_\Theta}{\tilde{\Theta}}.$$

Gradient model for special relativistic MHD [Carrasco+ 2020]

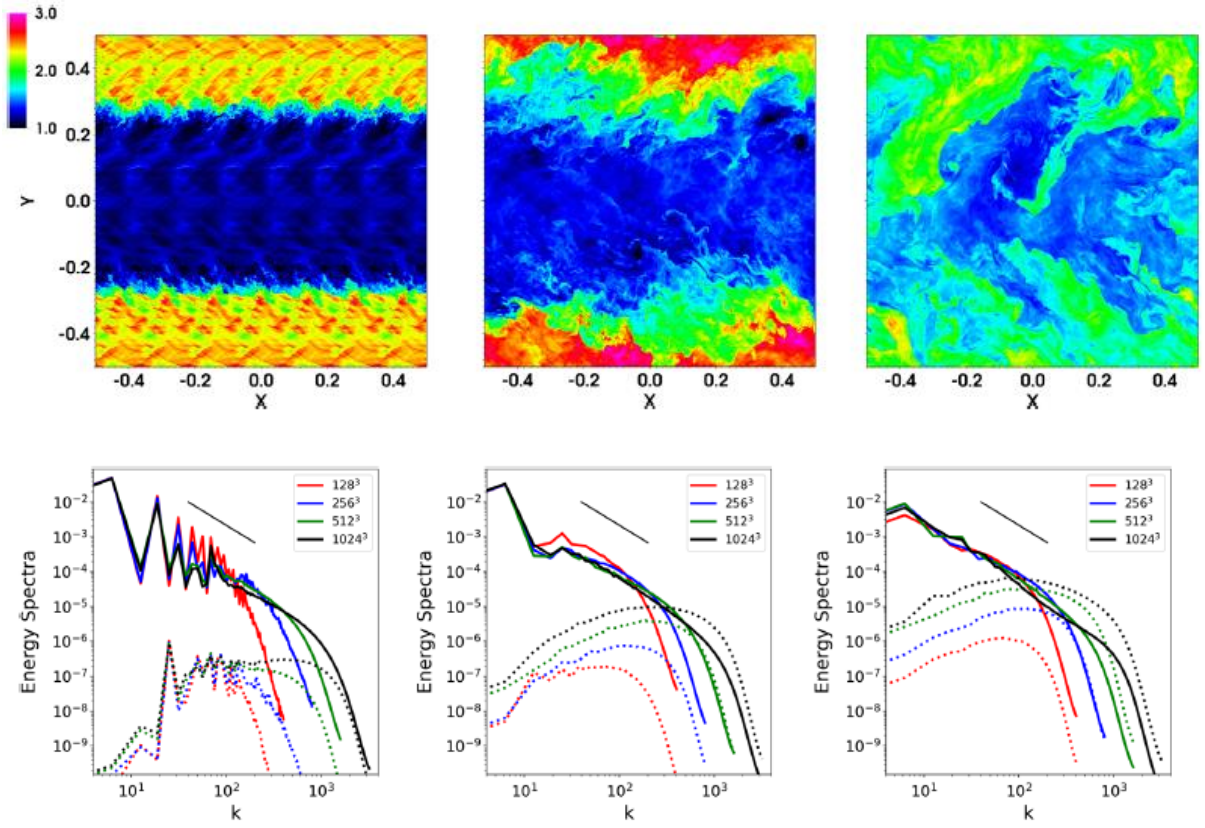

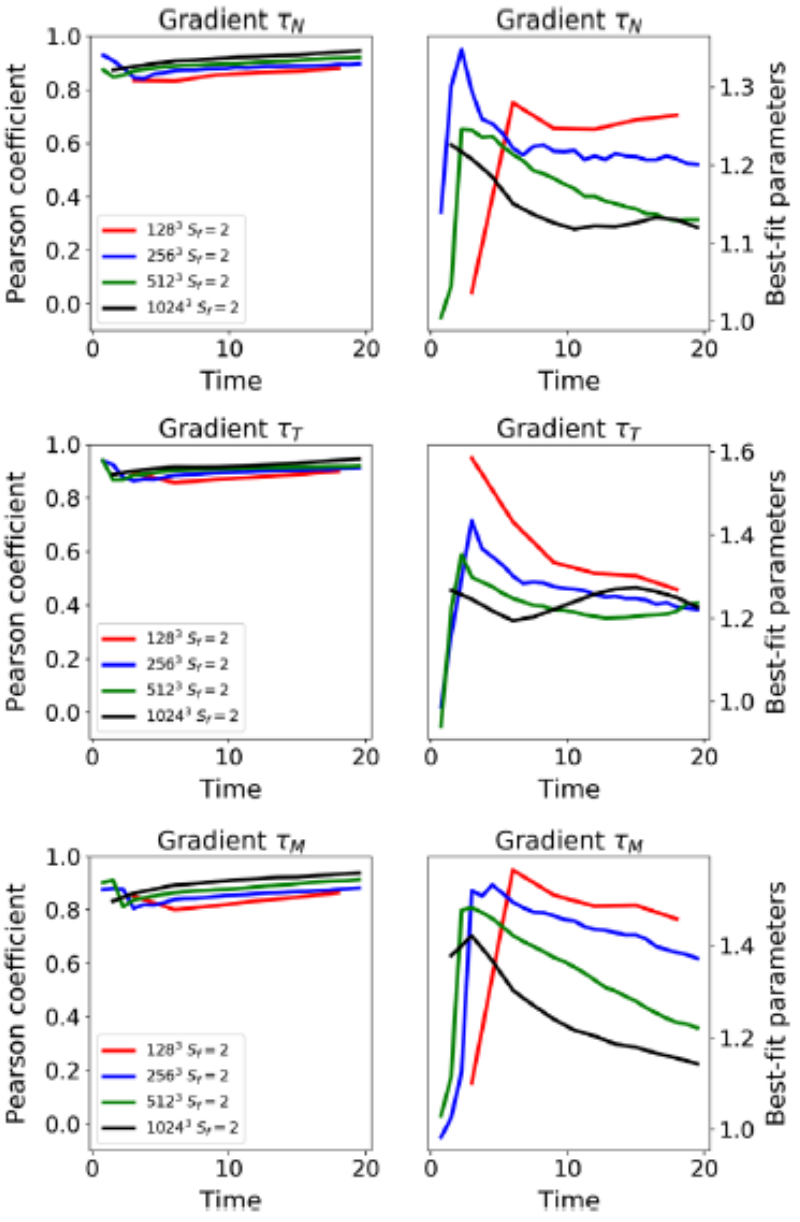

KHI box simulations, same behaviour as non-relativistic.

Excellent correlation SFS residuals-gradient model.

Gradient model for different filtering

[Carrasco+ 2020]

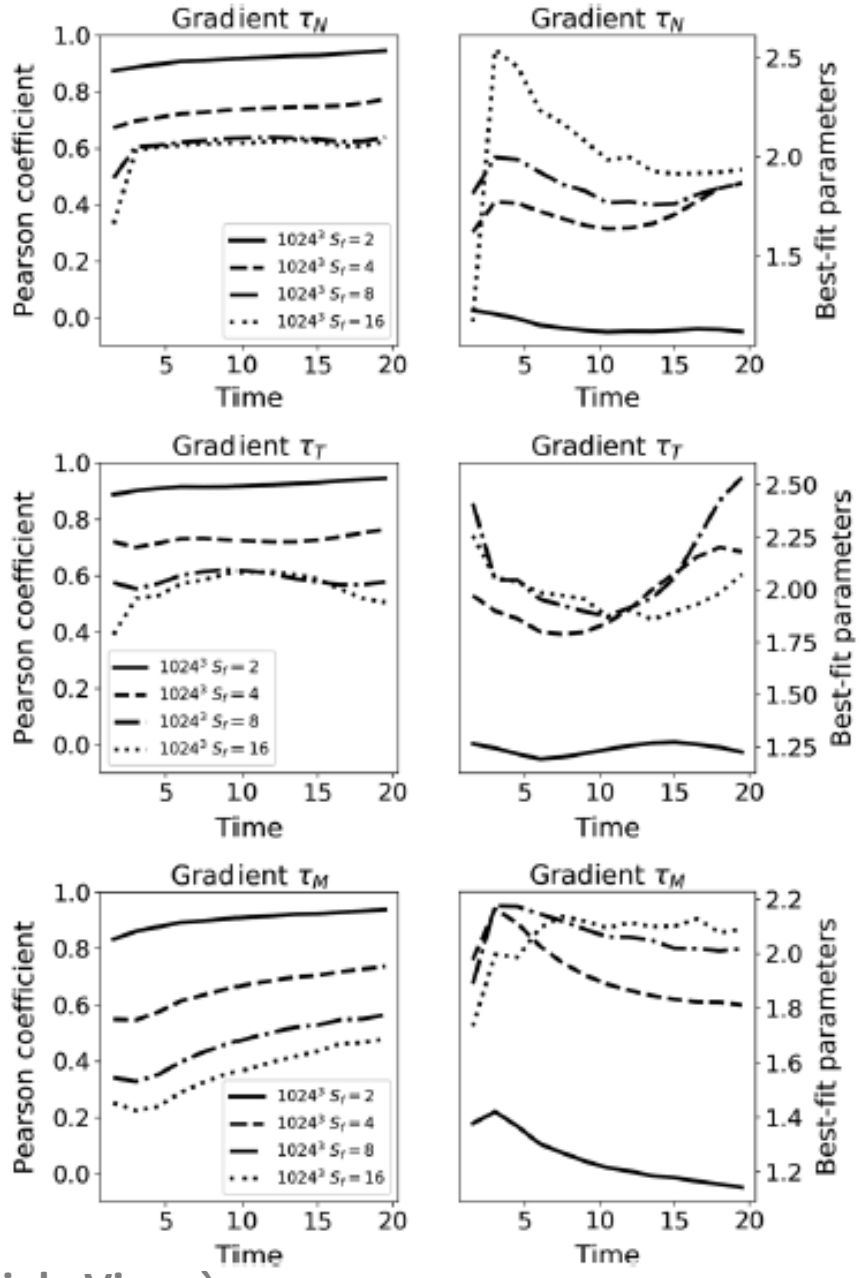

Higher filter: more information loss: more difficult to fit.

Applying the SGS gradient model partially includes the physics which would appear with an effective resolution higher by a factor of a few.

Gradient model for general relativistic MHD [Viganò+ 2020]

Assumptions & Caveats

- The space-time metric is not “turbulent”, i.e., the gradient terms arising from metric components in the fluid equations are neglected (verified by a-priori tests under typical conditions)
- Similarly, the SGS terms arising in the Einstein equations are not included, i.e., the steepness (derivatives) of MHD fields are dominating the non-linearity of the turbulence.
- The SGS modelling mimics the dynamics down to finite “depths” inside the cell: if physical dynamics qualitatively differ at much smaller scales, there is nothing one can do.
- The violation of covariance by adding SGS terms is negligible, since it is the same that happens when one discretizes the 3+1 equations with a certain numerical scheme (and in the continuous limit, there is no violation)

Gradient model for general relativistic MHD *[Viganò+ 2020]*

$$\partial_t(\sqrt{\gamma}\bar{D}) + \partial_k[-\beta^k\sqrt{\gamma}\bar{D} + \alpha\sqrt{\gamma}(\tilde{N}^k - \bar{\tau}_N^k)] = 0,$$
$$\partial_t(\sqrt{\gamma}\bar{S}_i) + \partial_k[-\beta^k\sqrt{\gamma}\bar{S}_i + \alpha\sqrt{\gamma}(\tilde{T}_i^k - \gamma_{ij}\bar{\tau}_T^{jk})] = \sqrt{\gamma}\overline{R^S}_i,$$
$$\partial_t(\sqrt{\gamma}\bar{U}) + \partial_k[-\beta^k\sqrt{\gamma}\bar{U} + \alpha\sqrt{\gamma}(\tilde{S}^k - \bar{\tau}_S^k)] = \sqrt{\gamma}\bar{R^U},$$
$$\partial_t(\sqrt{\gamma}\bar{B}^i) + \partial_k[\sqrt{\gamma}(-\beta^k\bar{B}^i + \beta^i\bar{B}^k) + \alpha\sqrt{\gamma}(\gamma^{ki}\bar{\phi} + \tilde{M}^{ki} - \bar{\tau}_M^{ki})] = \sqrt{\gamma}\overline{R_B}^i, \quad (20)$$

$$\partial_t(\sqrt{\gamma}\bar{\phi}) + \partial_k[-\beta^k\sqrt{\gamma}\bar{\phi} + \alpha c_h^2\sqrt{\gamma}\bar{B}^k] = \sqrt{\gamma}\overline{R^\phi}, \quad (21)$$

$$\tau_N^k = -C\xi H_N^k, \qquad \tau_T^{ki} = -C\xi H_T^{ki},$$
$$\tau_S^k = 0, \qquad \tau_M^{ki} = -C\xi H_M^{ki}.$$

The expressions are like in the Special Relativistic case, with the only difference that the gradient products symbolize spatial partial derivatives ∂i (and ∂j), with "·" indicating contraction among them with the spatial metric γij.

Gradient model for general relativistic MHD [Viganò+ 2020]

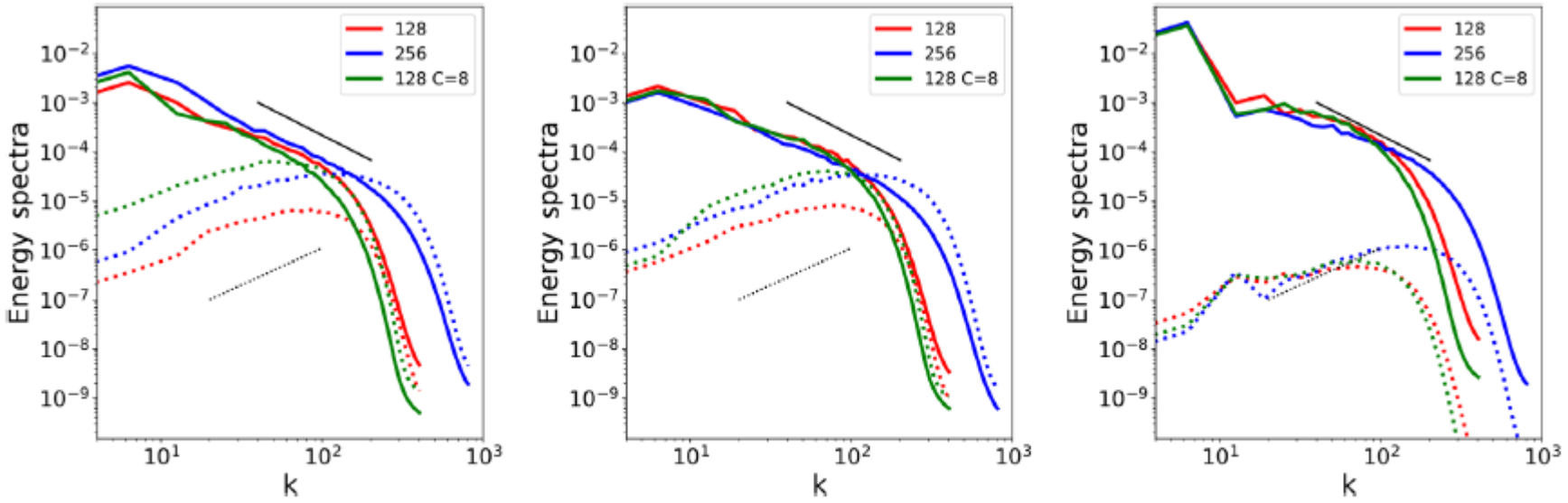

FIG. 6. Box simulations in 3D: *A posteriori* tests in curved background. Kinetic (solid lines) and magnetic (dashed lines) energy spectra at $t = 20$ for $\chi = 1$ (left panel), $\chi = [0.20 - 0.90]$ (middle panel), and $\chi = [0.20 - 0.24]$ (right panel) of a box simulation, compared with higher resolution and $\mathcal{C} = 8$.

We again find a-priori and a-posteriori excellent results, for a variety of fixed space-time backgrounds.

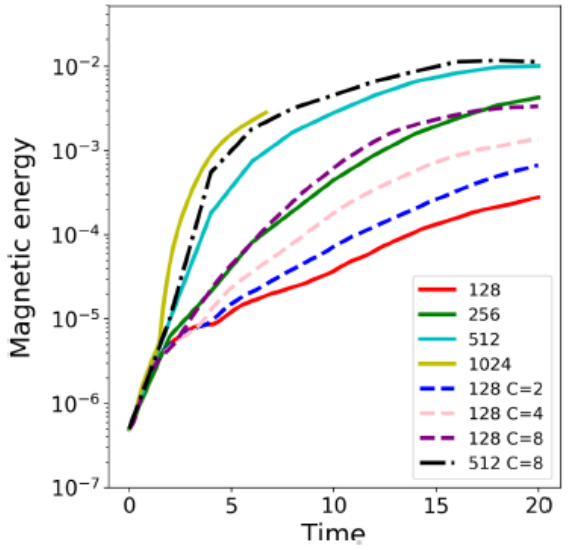

Simflowny code (developed by IAC3)

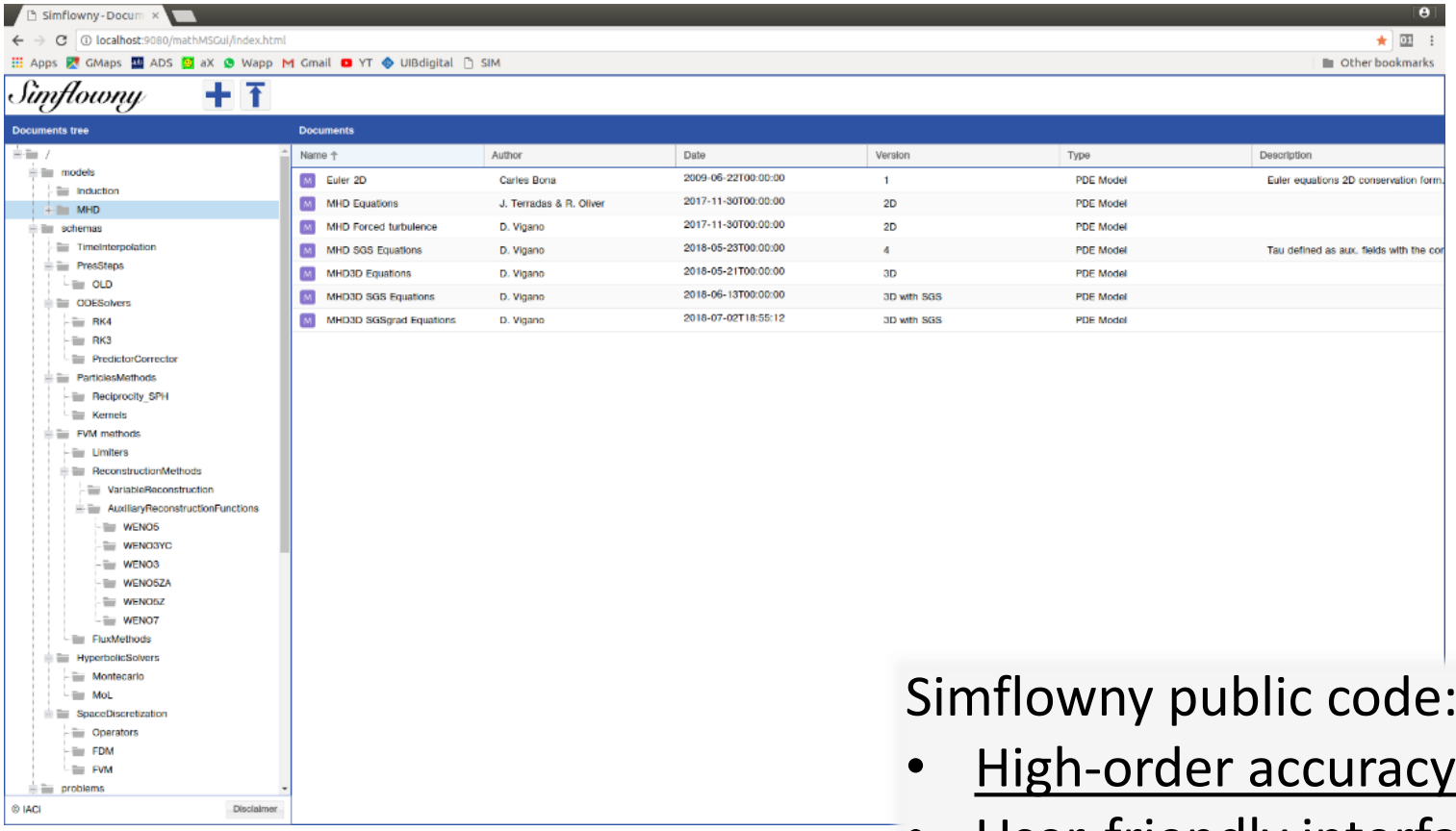

[Arbona+ 2018,
Palenzuela+ 2018,
Viganò+ 2019]

https://bitbucket.org/iac3/simflowny/

Simflowny public code:

- High-order accuracy methods
- User-friendly interface
- Modularity
- Any PDE
- Adaptive Mesh Refinement + Parallelization by SAMRAI

Methods & Models considered

[Aguilera-Miret+ 2020]

Einstein equation **4th order**
Kreiss-Oliger 6th order dissipation
Fluid MP5 reconstruction scheme + Lax-Friedrichs flux splitting formula
4th order differential operators for SGS terms
4th order Runge-Kutta

CCZ4 formulation of Einstein equations.
Initial data by Lorene, equal masses (1.3 Msun), quasi-circular orbits separated by 37 km
Magnetic fields initially **10^{11} G**, confined to each star
Hybrid EoS: piecewise Sly-like + ideal
Conversion to primitive via the more robust scheme by Kaustan+ 2020.
AMR (different resolutions) activated at merger time

Case	$\mathcal{C}_{\mathcal{M}}$	$\mathcal{C}_{\mathcal{T}} = \mathcal{C}_{\mathcal{N}}$	Refinement levels	Domain of finest grid (km)	Finest Δ (m)
C0 LR	0	0	5 FMR	[-35,35]	147
C0 MR	0	0	5 FMR+1 AMR	[-18,18]	74
C0 HR	0	0	5 FMR+2 AMR	[-9,9]	37
CM8	8	0	5 FMR	[-35,35]	147
CM8C1	8	1	5 FMR	[-35,35]	147
CM8C2	8	2	5 FMR	[-35,35]	147
CM8C4	8	4	5 FMR	[-35,35]	147
C8	8	8	5 FMR	[-35,35]	147

Low resolution

[Aguilera-Miret+ 2020]

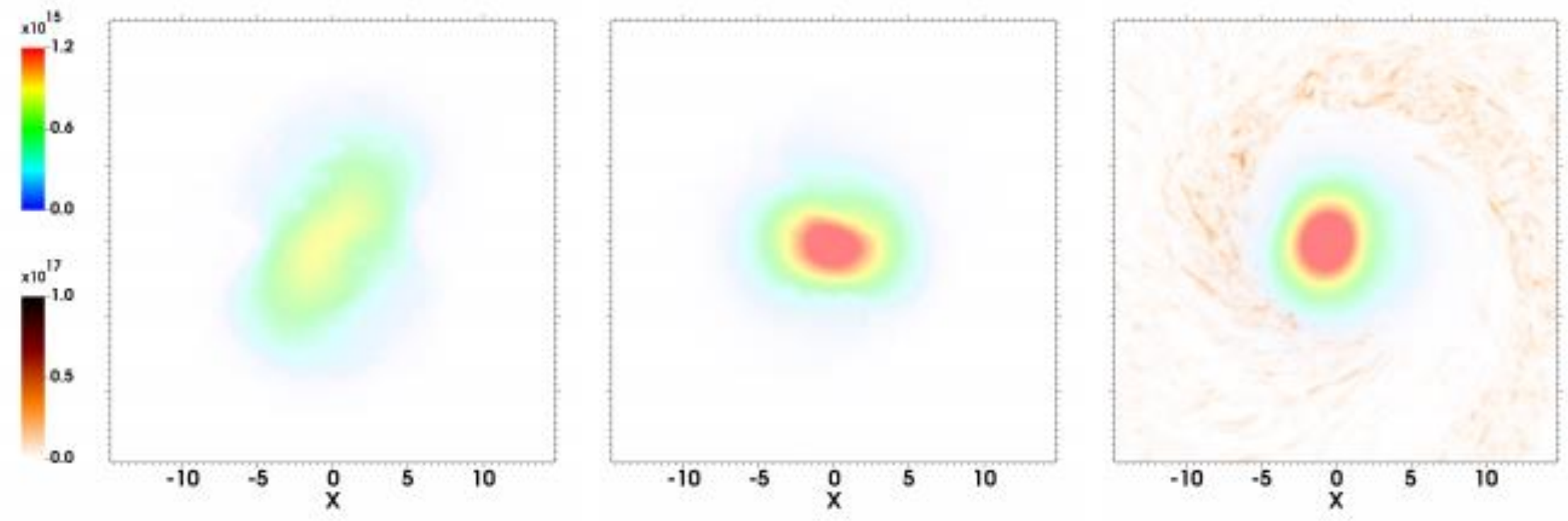

2.5 ms 5 ms 10 ms

Intermediate resolution

[Aguilera-Miret+ 2020]

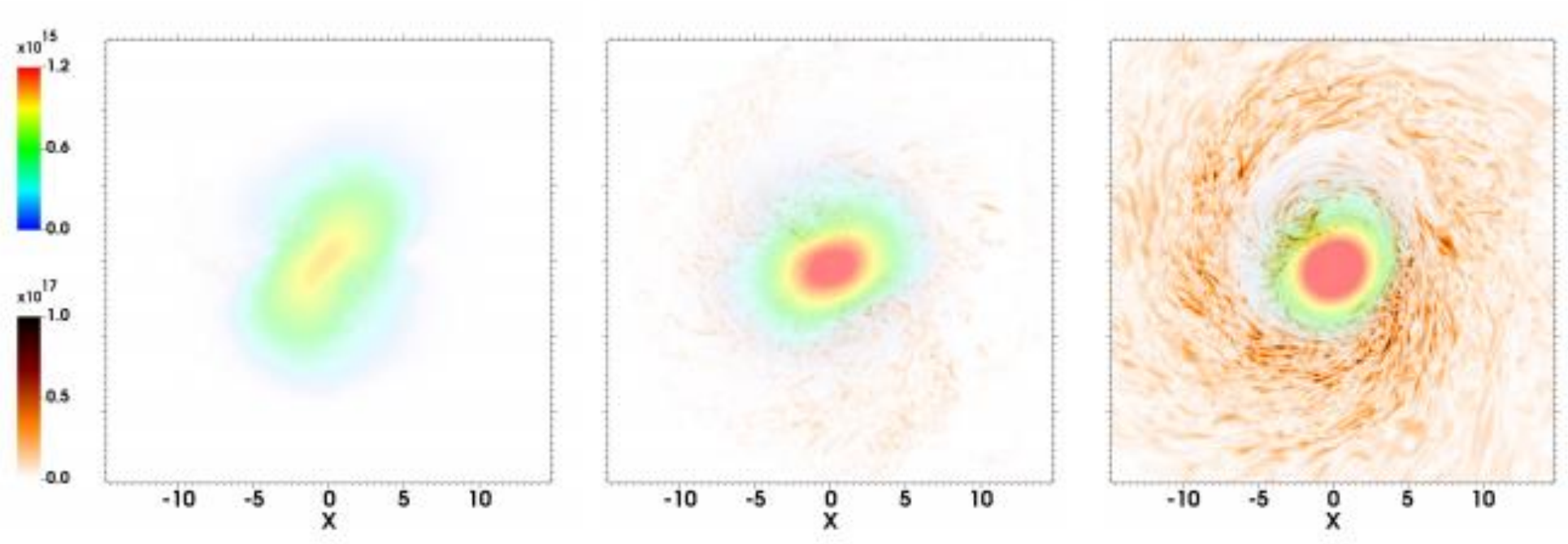

2.5 ms

5 ms

10 ms

High resolution

[Aguilera-Miret+ 2020]

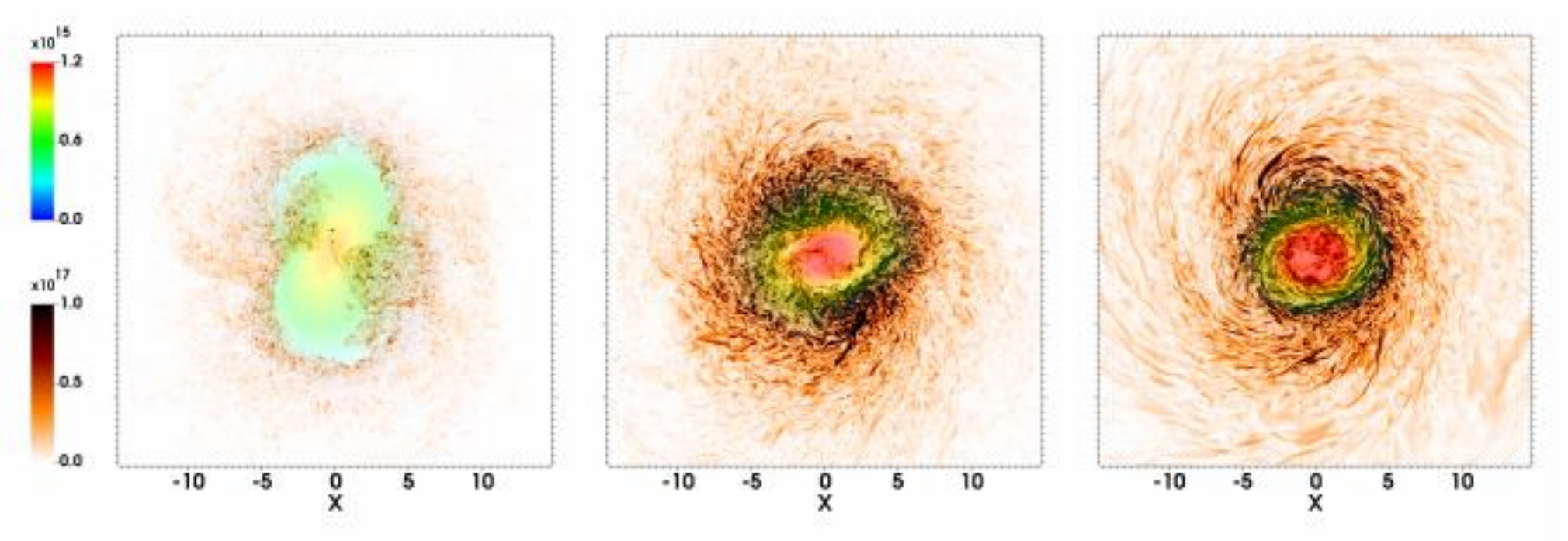

2.5 ms 5 ms 10 ms

Topology

[Aguilera-Miret+ 2020]

In the first 10 milliseconds, poloidal and toroidal fields are similar, but hints for the ordering of the toroidal fields by winding start to appear.

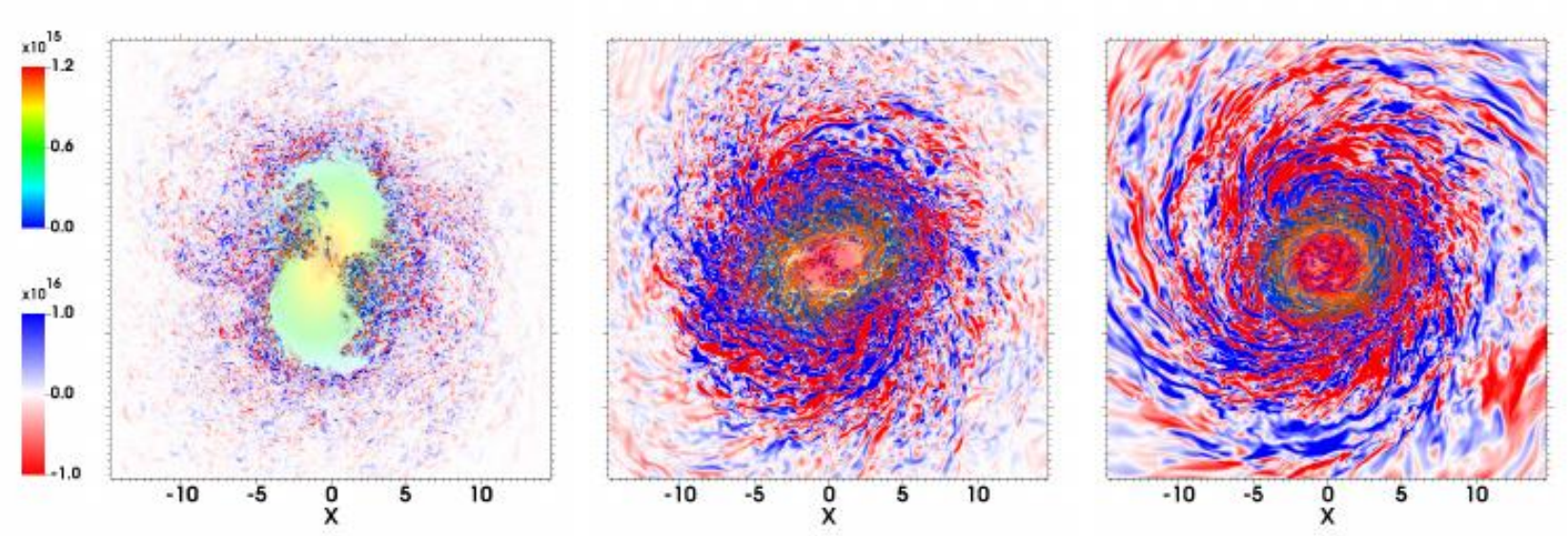

Amplification from 10^{11} G to 10^{17} G, small scales.

Topology

[Aguilera-Miret+ 2020]

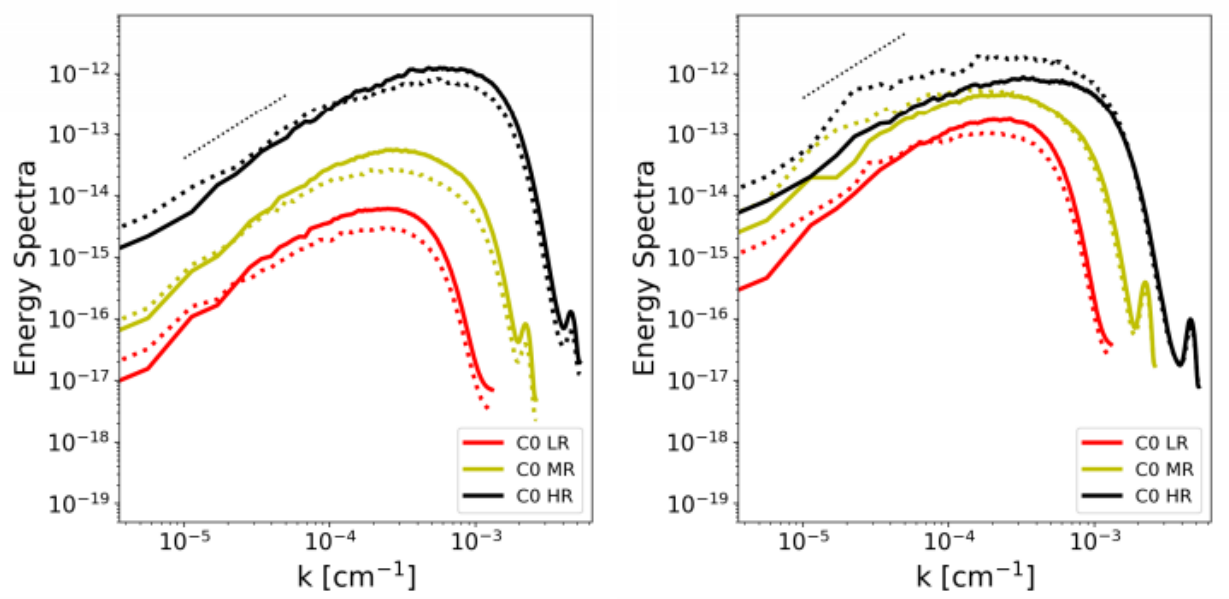

FIG. 4. *Magnetic energy spectra by components.* Magnetic poloidal (solid line) and toroidal (dashed line) spectra of `LR`, `MR` and `HR` cases at $t = 5\ ms$ (left) and $t = 10\ ms$ (right). The two components have similar profiles, although at $t = 10\ ms$ the toroidal component is slightly larger than the poloidal one for the high resolution cases `MR` and `HR`.

Low resolution + SGS model CM8

[Aguilera-Miret+ 2020]

LR

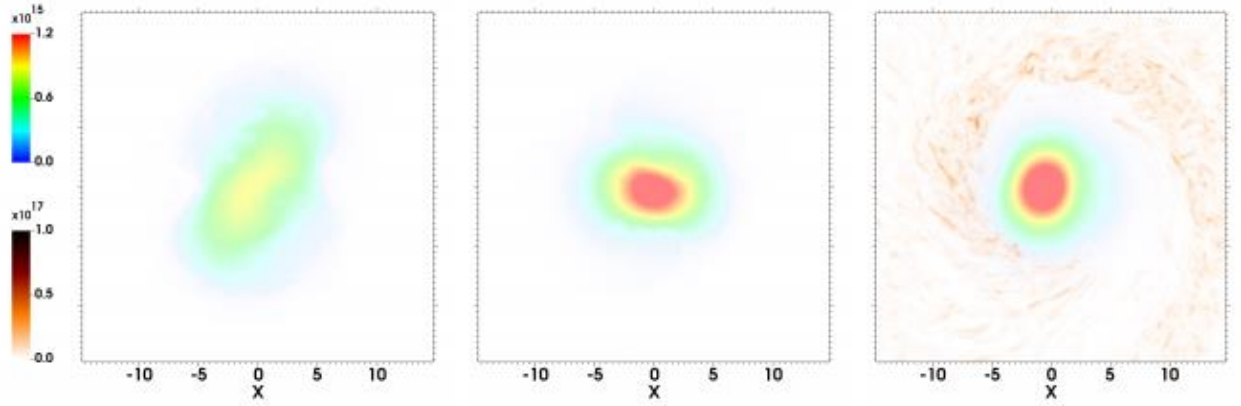

LR + SGS CM8

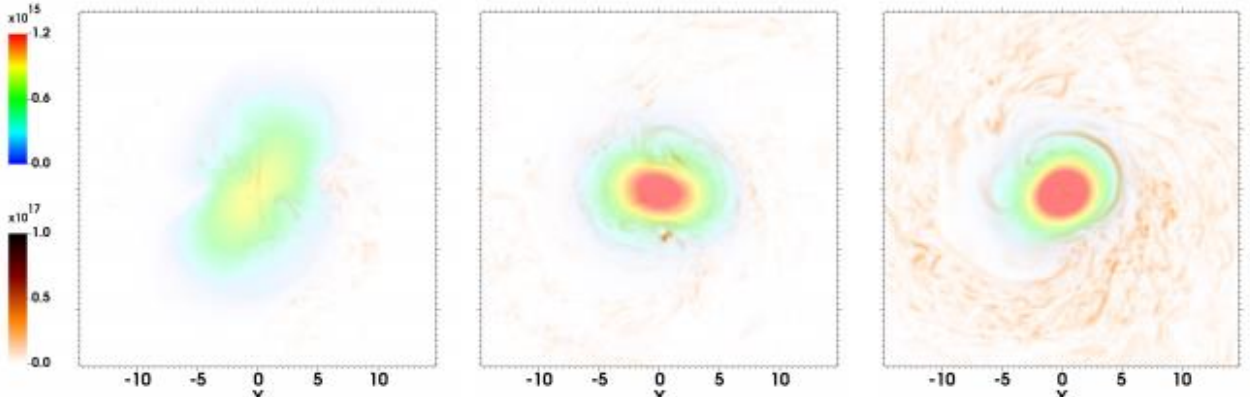

MR

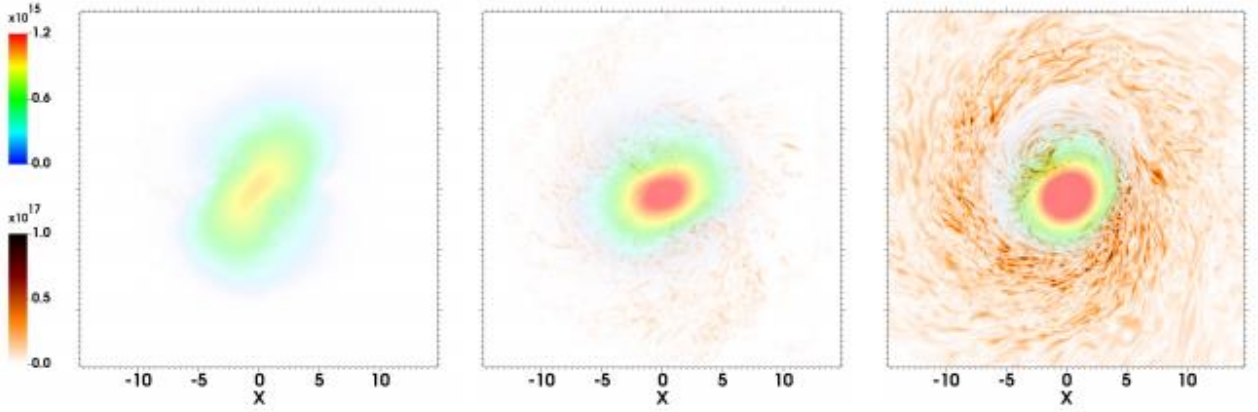

Comparison of magnetic amplification

[Aguilera-Miret+ 2020]

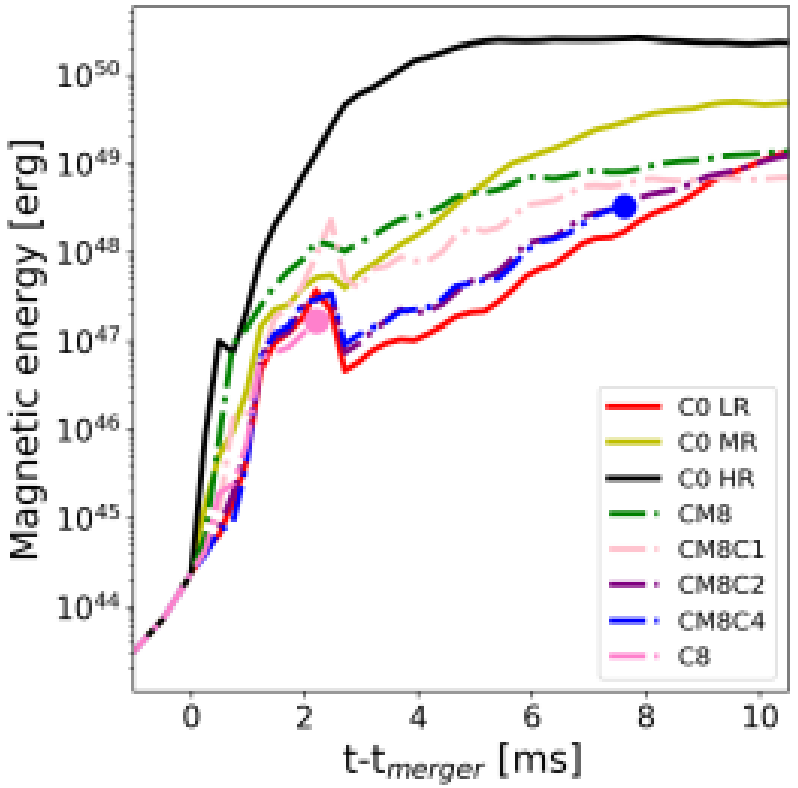

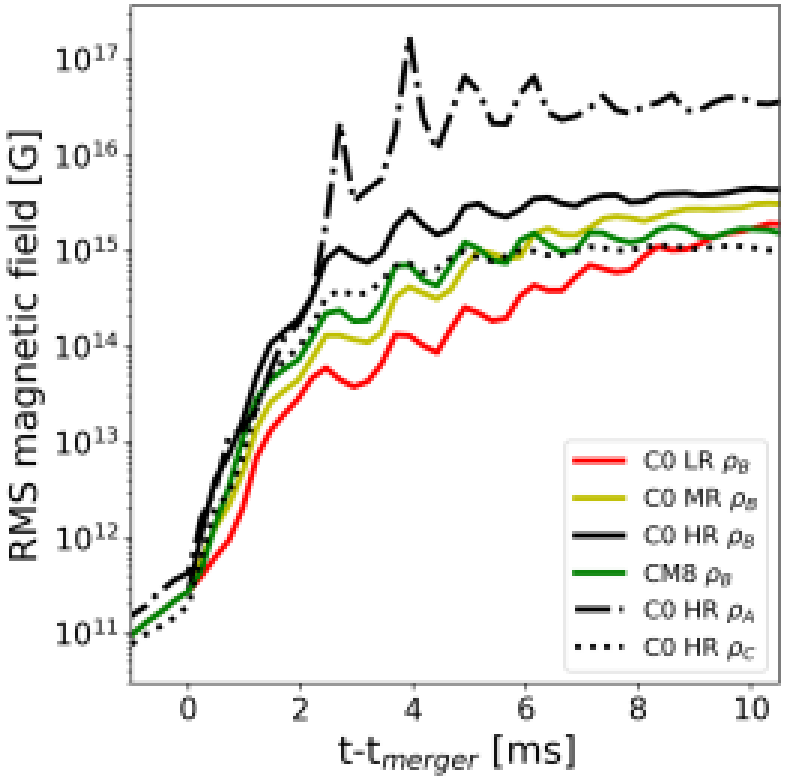

Non-linearity causes resolution/SGS-dependent collapse.
Effectiveness of SGS terms is evident mostly in the fast amplification phase.

Comparison of spectra

[Aguilera-Miret+ 2020]

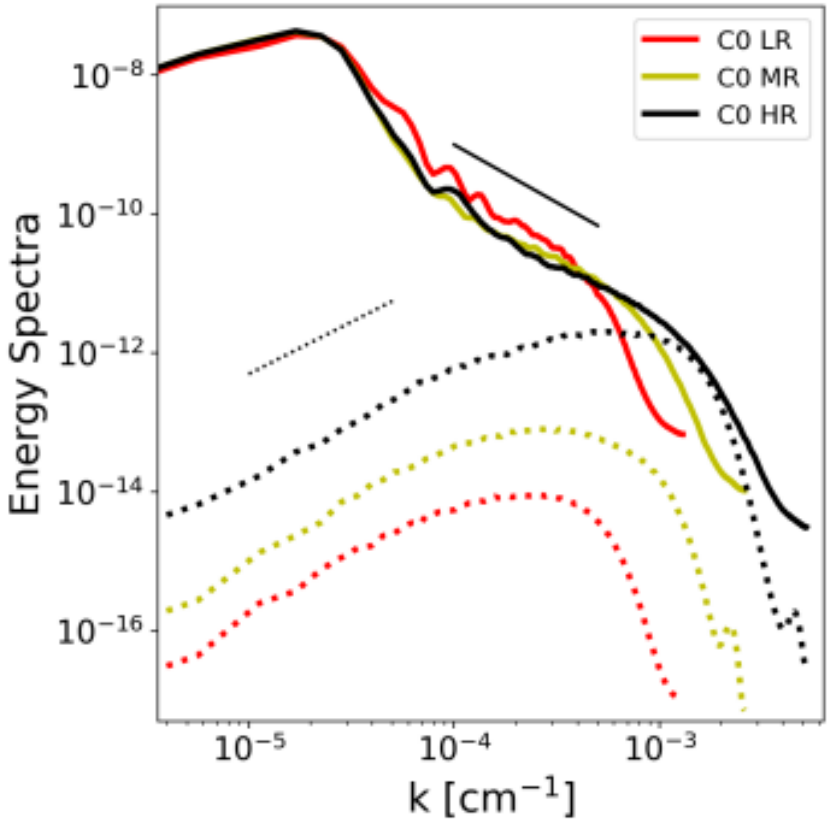

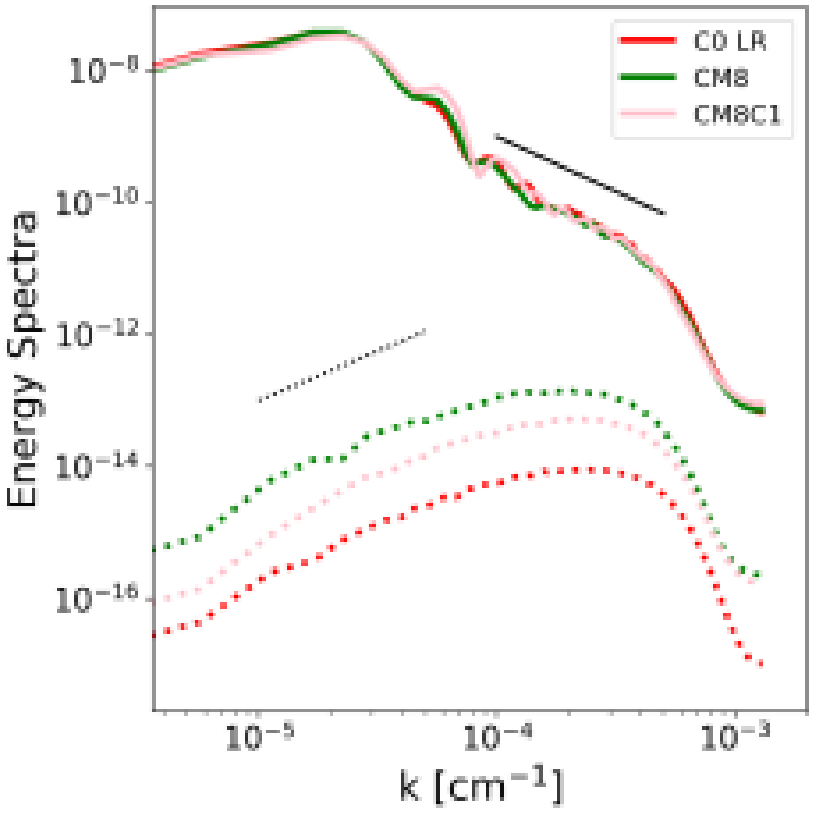

Spectra at 5 ms

Calibration issues

We found that the best results (closer to HR case) require:

- High values of C_M parameter (SGS in the induction equation)
- Zero or low values for C_T and C_N (continuity and momentum equations), otherwise turbulence is suppressed (excessive viscosity introduced?)

The reason could lie in the combined, non-trivial character of the SGS terms, which are also in part dissipative. By smoothing out the fluid, the dynamo is less efficient.

Need to investigate more!

Gravitational Waves

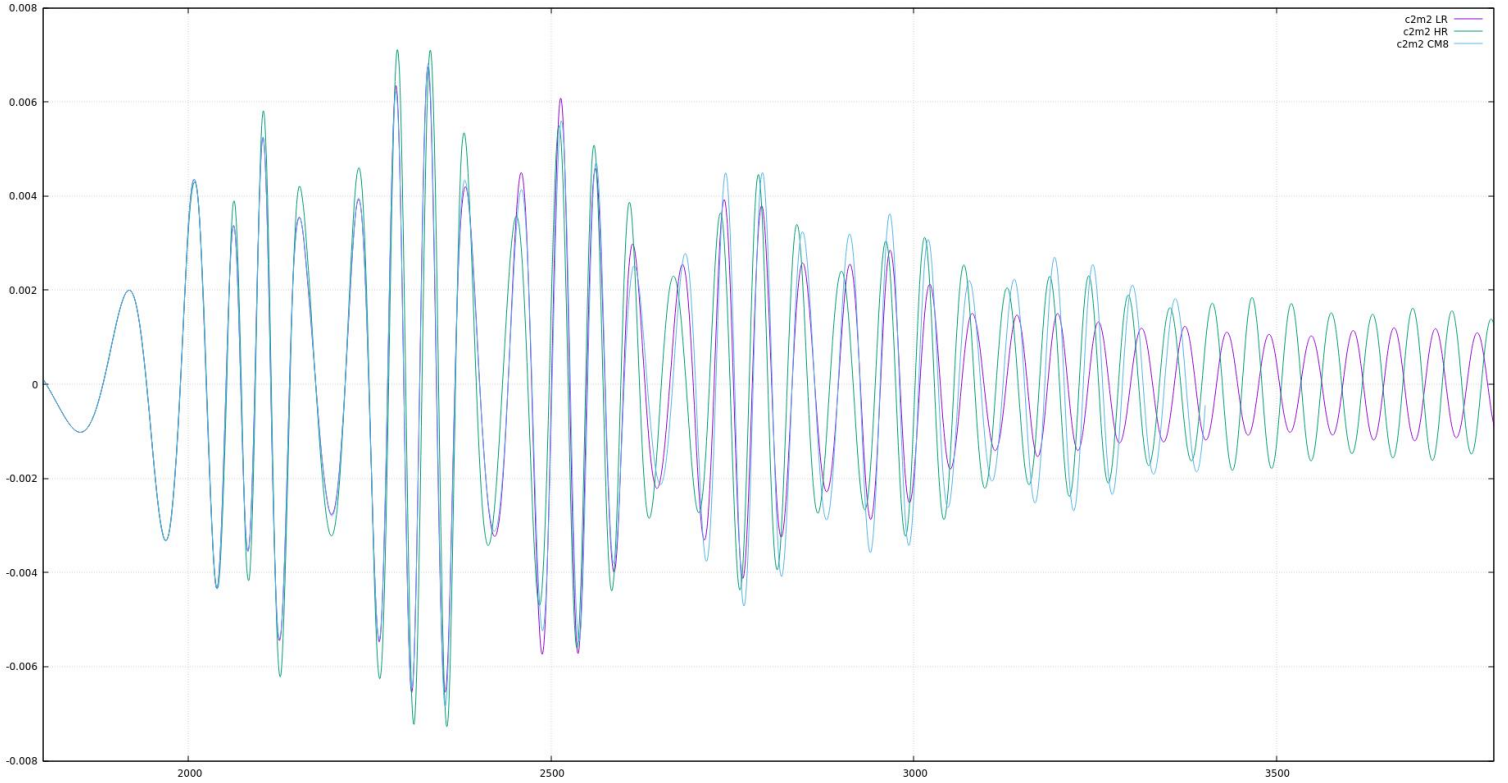

[Palenzuela+ in prep.]

Resolution/SGS effects are present in the post-merger only

Conclusions

1. Turbulent MHD in BNS cannot be fully captured numerically in the near future.
2. The magnetic configuration in a post-merger (after KHI) phase is turbulent, very far from a dipole and forgets about the initial seed topology.
3. The gradient model allows to include part of the unresolved dynamics, **saving of computational time** by one order of magnitude at least.
4. The “calibration” of the pre-coefficients is scheme-dependent and needs to be investigated further. However, a simple recipe including SGS terms in the induction equation only gives **interesting results for the amplification and a realistic topology**.
5. The formulation is general and **can be applied to BNS post-merger or any turbulent scenario.** Relevance to understand dynamo in general (for instance, formation of magnetars)

Numerical methods

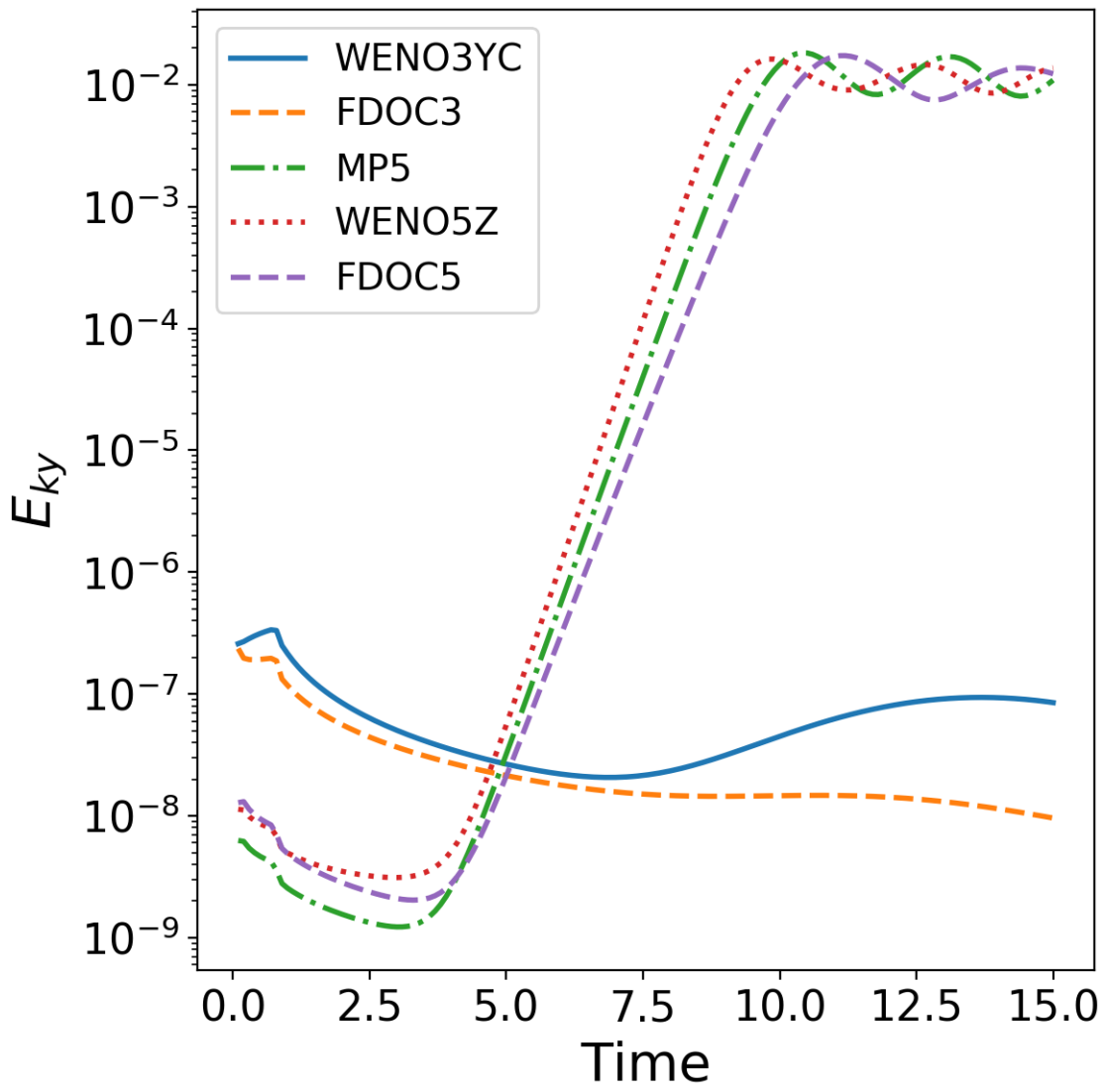

The growth rate depend on:

- physical problem (initial conditions, viscosity, eq. of state)
- numerical method (resolution, reconstruction)

Reproduced correct growth rates.

MP5 is the best choices for accuracy and stability.

[Palenzuela 2018+]